On the simultaneous cascades of energy, helicity, and enstrophy in incompressible homogeneous turbulence

P. Baj[1,2], F. Alves Portela[3,4] and D. W. Carter[4]†

[1]Department of Energy and Process Engineering, Norwegian University of Science and Technology, Trondheim, Norway

[2]Faculty of Power and Aeronautical Engineering, Warsaw University of Technology, Warsaw, Poland

[3]Univ. Lille, CNRS, ONERA, Arts et Metiers Institute of Technology, Centrale Lille, UMR 9014 - LMFL - Laboratoire de Mécanique des Fluides de Lille - Kampé de Fériet, F-59000 Lille, France

[4]Department of Aeronautical and Astronautical Engineering, University of Southampton, Southampton, UK

(Received xx; revised xx; accepted xx)

We characterise the incompressible turbulence cascade in terms of the concurrent inter-scale and inter-space exchanges of the scale-by-scale energy, helicity and enstrophy. The governing equations for the scale-by-scale helicity and enstrophy are derived in a similar fashion to that of the second order structure function following Hill (2002). We examine the instantaneous dynamics that establish the statistically steady state by applying these equations to both forced periodic turbulence and a von Kármán flow, and focusing on scales in the dissipative range $r = 2.5\eta$, the near-dissipative range $r = 0.5\lambda$ and the onset inertial range $r = \lambda$ (where η and λ are the Kolmogorov and Taylor length scales, respectively). It is found that the instantaneous mechanisms in those equations are correlated both within and across the energy, enstrophy and helicity transfers. The signature of the random sweeping effect is observed in all three individual budgets and between the energy and enstrophy transfers. The anti-correlation of the pressure transport and non-linear transfer, previously established in the energy cascade, is found to hold also in the helicity cascade. Owing to its lack of positive definiteness, the helicity transfers are found to be decorrelated from the others. However a connection between the energy cascade and helicity is identified kinematically. This connection reveals the large-scale sweeping motions captured by the two-point velocity sum $\Sigma u_i = u_i + u_i'$ as a key element in the overall energy cascade and underpins previous observations of large-scale intermittency. Taken together, this work extends a classic framework to gain novel insight on turbulence dynamics that underlay the statistically steady state, and demonstrates how transfers are interconnected.

1. Introduction

Turbulence is an inherently multi-scale phenomenon arising from the non-linear nature of the motion of fluids. In general, a turbulent flow is populated by a hierarchy of eddies, the largest of which appear through interactions between the fluid and its boundaries (or some explicit forcing) and the smallest being conditioned by viscous forces (Falkovich 2009), with energy flowing, on average, from the former to the latter. This

† Email address for correspondence: D.W.Carter@soton.ac.uk

statistical picture of turbulence is described by the so-called Richardson-Kolmogorov cascade (Richardson 1920; Kolmogorov 1941*a*,*b*). However, this cascade is a result of dynamic interactions between eddies of various sizes (Pelz *et al.* 1985). The distinction between the instantaneous interactions in the turbulence and the statistically stationary cascade that they give rise to are a well known problem in turbulence modelling. For example, in Large Eddy Simulations (LES) the directionality of the cascade at any given instant cannot be predicted from statistically stationary models (Germano *et al.* 1991; Alexakis & Chibbaro 2020). Recent work by Goto & Vassilicos (2016) and Yasuda & Vassilicos (2018) highlights how viewing the cascade from a statistically stationary viewpoint overlooks important dynamics that determine how such a stationary state itself is established. The present work seeks to expand on that perspective by analysing the concurrent scale-by-scale budgets of energy, helicity and enstrophy by deriving the equations governing those cascades directly from the Navier-Stokes equations, NS, without any averaging or statistical assumptions. We then apply these equations to two distinct homogeneous turbulent flows: forced periodic turbulence and a von Kármán flow.

The kinetic energy $q^2 = \frac{1}{2}\boldsymbol{u}\cdot\boldsymbol{u}$ is a central quantity in characterising turbulent flows and it has been, historically, at the core of theories of turbulence. Away from any boundaries, q^2 can only be destroyed by the turbulent dissipation ε arising from small scale motions in the fluid (i.e. in the absence of viscosity q^2 is a conserved quantity of the Navier-Stokes equations). Indeed, in the classical theory of Kolmogorov (1941*b*), where the details of the largest scales are dispensed with, the turbulence cascade is formulated in terms of a budget for δq^2, representing, to a large extent (Davidson & Pearson 2005), the energy density at a given scale r. This energy cascade is governed solely by the non-linear transfer of δq^2 from large to small scales which is in equilibrium with ε. Under the assumptions of homogeneity and isotropy, Kolmogorov closed the relationship between q^2 and ε through the 4/5-ths law leading to the inertial-scale distribution $\delta q^2 \sim r^{2/3}$ (the 5/3-rds law for the energy spectrum), practically ubiquitous with turbulence (Kraichnan 1974).

In fact, ε arises due to the finest structures in the turbulence that are characterised by strong vorticity $\boldsymbol{\omega} = \nabla \times \boldsymbol{u}$ and therefore large enstrophy $\omega^2 = \boldsymbol{\omega}\cdot\boldsymbol{\omega}$. While dynamically distinct (see discussion of Carbone & Bragg 2020), it can be shown that the dissipation and enstrophy are closely related (Raynal 1996) upon integration over all space (Tsinober 2001; Tennekes & Lumley 2018). Enstrophy exhibits its own cascade across scales but, due to the presence of vortex stretching, this cascade is not inviscidly conservative. Indeed, it is known since the work of Fjørtoft (1953) that in two dimensions (i.e. in the absence of vortex stretching), enstrophy cascades from large to small scales, effectively reversing the direction of the energy cascade (Eyink 1996; Kraichnan 1967). Although purely two-dimensional flows are seldom realised in nature, such an idealised cascade is an important element in our understanding of a variety of turbulent flows (see reviews by Boffetta & Ecke 2012; Falkovich *et al.* 2017) as would be the case of geostrophic flows (Lindborg 2007; Lindborg & Nordmark 2022), strongly rotating turbulence (Deusebio *et al.* 2014; van Kan & Alexakis 2022) but also in flows that exhibit coherent structures (Dascaliuc & Grujić 2013). Recently, Bos (2021) analysed three-dimensional turbulence, where vortex stretching is suppressed altogether; they found that enstrophy is preserved but energy is not and showed how this modified system displayed a dual direct cascade of both energy (no longer inviscidly conserved) and enstrophy.

Vorticity also features in the helicity $h = \boldsymbol{u}\cdot\boldsymbol{\omega}$, which is another inviscid invariant of the Navier-Stokes equations, and acts as a measure of breakage in mirror-symmetry, or parity-invariance, within the fluid (Moreau 1960; Moffatt 1969). Topologically, it describes the degree of knottedness of vortex tubes (Moffatt & Tsinober 1992) a concept which is quite useful in the study of superfluid turbulence, where very large Reynolds numbers can be achieved (see e.g. Kivotides & Leonard 2021; Kleckner *et al.* 2016). As noted by Brissaud *et al.* (1973), because h is not positive definite (as are q^2 and ω^2) the possibility of a dual direct cascade exists in tandem with that of one analogous to the two-dimensional scenario described above (see also Kraichnan 1973). It is established that the most physically sound scenario is that of a dual (direct) cascade (see e.g. Chen *et al.* 2003). The bulk of the work on helicity cascades has been carried out in Fourier space (see Scott & Wang 2005; Alexakis 2017; Alexakis & Biferale 2018; Pouquet *et al.* 2019) where the non-linearity of the Navier-Stokes equations is more easily described by triad interactions of wavenumbers (as motivated by Waleffe 1992) at the sacrifice of requiring homogeneity. For flows in which some degree of anisotropy or inhomogeneity is present, non-zero helicity can give rise to the spontaneous formation of large-scale coherence in the flow (see Yokoi & Yoshizawa 1993, and references therein). Their effect on the cascade is likely non-trivial.

Recognising that the Richardson-Kolmogorov cascade is insufficient for a general description of turbulence, Hill (2002) derived a budget for δq^2 that reduces to that of Kolmogorov (under the assumptions of homogeneity, isotropy, and stationarity) but is instead obtained directly from the Navier-Stokes equations without requiring any information regarding the structure of the flow or the Reynolds number. This equation, often referred to as the generalised Kolmogorov equation (Mollicone *et al.* 2018; Gatti *et al.* 2020) or the Kármán-Howarth-Monin-Hill equation (Alves Portela *et al.* 2017; Yasuda & Vassilicos 2018), characterises the energy cascade in terms of physical and scale space exchanges of δq^2 (as well as any sources or sinks) such that the non-linear transfer of δq^2 is but one of the mechanisms in balance with ε, which always acts as a sink of δq^2. In recent years, this equation has been extensively used to characterise the effects of inhomogeneity and anisotropy on the energy cascade (Gomes-Fernandes *et al.* 2015; Cimarelli *et al.* 2016; Knutsen *et al.* 2020; Zimmerman *et al.* 2022) and has been extended to variable density and compressible flows (Lai *et al.* 2018; Arun *et al.* 2021).

It is clear that a full characterisation of the turbulence cascade must involve not only the turbulent kinetic energy but also quantities such as enstrophy and helicity, as they bear relation to dissipation (a core element of the energy cascade) and capture the presence of coherence, intermittency, and other such phenomena that are known to break with the classical picture of turbulence. Following this observation, the objectives of the present study are threefold:

(i) To provide a generalised framework for analysing the transfers of energy, enstrophy and helicity through two-point equations for these quantities, following Hill (2002).
(ii) To combine this framework with the correlation-based analysis of the energy transfers (Yasuda & Vassilicos 2018), examining how the different mechanisms involved in the scale-by-space energy, helicity, and enstrophy budgets are related.
(iii) To leverage the two-point framework towards a deeper understanding of the connection between the instantaneous energy cascade and helicity.

We begin with the formal derivation of the scale-space equations in section 2. A brief description and characterisation of the data sets on which the scale-space equations will be applied is given in section 3. The correlations between the individual terms of each of the three transfer budgets is shown in section 4. In section 5 we discuss the role played by helicity in the energy cascade from a two-point scale-by-scale perspective. We conclude with a summary of our results and suggestions for future work in section 6.

2. Formulation

The single-point quantities of interest that will be cast into the scale-space framework are the energy q^2, helicity h, and enstrophy ω^2. The formulation begins with the familiar single-point incompressible Navier-Stokes (NS) equations:

$$\frac{\partial}{\partial t}u_i + u_k\frac{\partial u_i}{\partial x_k} = -\frac{1}{\rho}\frac{\partial p}{\partial x_i} + \nu\frac{\partial^2 u_i}{\partial x_k \partial x_k} \tag{2.1}$$

together with the incompressibility condition $\nabla \cdot \boldsymbol{u} = 0$ where $u_i(\boldsymbol{x}, t)$ and $p(\boldsymbol{x}, t)$ are the instantaneous velocity and pressure fields, respectively, with ν the kinematic viscosity and ρ the density. In addition to eq. (2.1) the vorticity form of the NS equations is invoked taking the curl:

$$\frac{\partial}{\partial t}\omega_i + u_k\frac{\partial \omega_i}{\partial x_k} = \omega_k\frac{\partial u_i}{\partial x_k} + \nu\frac{\partial^2 \omega_i}{\partial x_k \partial x_k} \tag{2.2}$$

where $\boldsymbol{\omega} = \nabla \times \boldsymbol{u}$ is the vorticity with the kinematic property $\nabla \cdot \boldsymbol{\omega} = 0$.

2.1. *Generalised scale to scale transfers*

In this section we outline the general method for obtaining the scale-space energy, helicity, and enstrophy budget equations. These originate from studies focused on the energy and can be found in the classic work of Von Karman & Howarth (1938) and later made general in order to account for anisotropy (Monin & Yaglom 1975) and inhomogeneity (Hill 2002). As such the evolution equations are commonly referred to as the generalised Kármán-Howarth-Monin (KHM) equations or the Kármán-Howarth-Monin-Hill (KHMH) equations. For the present work, these equations will be used to describe the scale-space dynamics of three specific structure functions: the energy structure function $\delta q^2 = \delta u_i \delta u_i$, the helicity structure function $\delta h = \delta u_i \delta \omega_i$, and the enstrophy structure function $\delta \omega^2 = \delta \omega_i \delta \omega_i$. Here, δu_i and $\delta \omega_i$ represent, respectively, velocity and vorticity increments, taken as the difference of that quantity at two points x_i and x'_i i.e. $\delta u_i = u_i - u'_i$ and $\delta \omega_i = \omega_i - \omega'_i$. Henceforth, primed variables denote belonging to a set of spatial points x'_i independent of x_i. A detailed derivation and interpretation of the KHMH equations in the scale-space coordinates system is given in Hill (2002) and Marati *et al.* (2004). In the present study we abstain from using the Reynolds decomposition instead following a similar approach to Yasuda & Vassilicos (2018) where the instantaneous dynamics of each term at various scales can be analysed.

The derivation of the transfer equations begins with the equations for velocity and vorticity, eq. (2.1) and eq. (2.2). There are three common steps in deriving the budgets for δq^2, δh, and $\delta \omega^2$:

(i) Take the difference of eq. (2.1) and eq. (2.2) evaluated on two independent coordinates x_k and x'_k. These constitute the two-point equations for the velocity and vorticity differences ($\delta u_i = u_i - u'_i$ and $\delta \omega_i = \omega_i - \omega'_i$, respectively)

- (*a*) For δq^2: Multiply the equation for δu_i by $2\delta u_i$.
- (*b*) For δh: Add the product between $\delta \omega_i$ and the equation for δu_i to the product between δu_i and the equation for $\delta \omega_i$.
- (*c*) For $\delta \omega^2$: Multiply the equation for $\delta \omega_i$ by $2\delta \omega_i$.

(ii) Express all quantities as two-point differences (δ) or sums (Σ). The strain rate tensor, that appears in the equation for $\delta\omega^2$, is expressed as $S_{ik} = \frac{1}{2}\left(\frac{\partial u_i}{\partial x_k} + \frac{\partial u_k}{\partial x_i}\right)$ with $\delta S_{ik} = S_{ik} - S'_{ik}$ and $\Sigma S_{ik} = S_{ik} + S'_{ik}$.

(iii) Change the coordinate system from (x_k, x'_k) to (X_k, r_k), where $X_k \equiv \frac{1}{2}(x_k + x'_k)$ represents physical space (in the sense that it represents a centroid position) and $r_k \equiv x'_k - x_k$ represents the space of scales (as it relates to a distance vector).

The resulting equations describe the various budgets of the scale-space energy, helicity, and enstrophy structure functions. For the energy structure function δq^2 one obtains:

$$\begin{aligned} \frac{\partial}{\partial t}\delta q^2 + \frac{\partial \delta u_k \delta q^2}{\partial r_k} &= -\frac{\partial}{\partial X_k}\Big(\frac{\Sigma u_k \delta q^2}{2}\Big) - \frac{2}{\rho}\frac{\partial \delta u_k \delta p}{\partial X_k} \\ &+\nu\Big[2\frac{\partial^2}{\partial r_k^2} + \frac{1}{2}\frac{\partial^2}{\partial X_k^2}\Big]\delta q^2 - 2\nu\Big[\Big(\frac{\partial u_i}{\partial x_k}\Big)^2 + \Big(\frac{\partial u'_i}{\partial x'_k}\Big)^2\Big] \end{aligned} . \tag{2.3}$$

In shorthand notation:

$$\mathcal{A}_t^{q^2} + \Pi^{q^2} = -\mathcal{T}^{q^2} - \mathcal{T}_p^{q^2} + \mathcal{D}_\nu^{q^2} - \mathcal{E}^{q^2} \tag{2.4}$$

where the superscript denotes the energy q^2 and the terms of eq. (2.4) reflect the terms presented in eq. (2.3) sequentially. For the helicity structure function δh one obtains:

$$\begin{aligned} \frac{\partial}{\partial t}\delta h + \frac{\partial}{\partial r_k}\Big[\delta u_k \delta h - \frac{1}{2}\delta\omega_k \delta q^2\Big] &= -\frac{\partial}{\partial X_k}\Big[\frac{\Sigma u_k \delta h}{2} - \frac{\Sigma \omega_k \delta q^2}{4}\Big] \\ -\frac{1}{\rho}\frac{\partial \delta\omega_k \delta p}{\partial X_k} + \nu\Big[2\frac{\partial^2}{\partial r_k^2} + \frac{1}{2}\frac{\partial^2}{\partial X_k^2}\Big]\delta h &- 2\nu\Big[\Big(\frac{\partial \omega_i}{\partial x_k}\frac{\partial u_i}{\partial x_k}\Big) + \Big(\frac{\partial \omega'_i}{\partial x'_k}\frac{\partial u'_i}{\partial x'_k}\Big)\Big]. \end{aligned} \tag{2.5}$$

In shorthand notation:

$$\mathcal{A}_t^{h} + \Pi^{h} = -\mathcal{T}^{h} - \mathcal{T}_p^{h} + \mathcal{D}_\nu^{h} - \mathcal{E}^{h} \tag{2.6}$$

where the superscript denotes the helicity h for the respective terms of eq. (2.5). Finally, for the enstrophy $\delta\omega^2$ one obtains:

$$\begin{aligned} \frac{\partial}{\partial t}\delta\omega^2 + \frac{\partial \delta u_k \delta\omega^2}{\partial r_k} &= -\frac{\partial}{\partial X_k}\Big(\frac{\Sigma u_k \delta\omega^2}{2}\Big) + (\delta\omega_k\delta\omega_i\Sigma S_{ik} + \Sigma\omega_k\delta\omega_i\delta S_{ik}) \\ &+\nu\Big[2\frac{\partial^2}{\partial r_k^2} + \frac{1}{2}\frac{\partial^2}{\partial X_k^2}\Big]\delta\omega^2 - 2\nu\Big[\Big(\frac{\partial \omega_i}{\partial x_k}\Big)^2 + \Big(\frac{\partial \omega'_i}{\partial x'_k}\Big)^2\Big]. \end{aligned} \tag{2.7}$$

In shorthand notation:

$$\mathcal{A}_t^{\omega^2} + \Pi^{\omega^2} = -\mathcal{T}^{\omega^2} + \mathcal{G}_S^{\omega^2} + \mathcal{D}_\nu^{\omega^2} - \mathcal{E}^{\omega^2} \tag{2.8}$$

where the superscript denotes the enstrophy ω^2.

Notice that these three budgets are similarly structured, where:

- $\mathcal{A}_t$ is an unsteady term and represents the temporal increase or decrease of scale energy/helicity/enstrophy at each instant.

- Π represents the non-linear exchanges in scale space of energy/helicity/enstrophy.
- $\mathcal{T}$ is the nonlinear turbulent transport in physical space.
- $\mathcal{T}_p$ results from the interaction of the pressure and velocity/vorticity fields to produce a pressure transport that acts to transport energy/helicity at a particular scale.
- $\mathcal{G}_S$ Is a generation term in scale space resulting from the coupling between the rate-of-strain and the enstrophy.
- $\mathcal{D}_\nu$ represents the viscous diffusion of energy/helicity/enstrophy both in scale and physical space.
- $\mathcal{E}$ represents the two-point average dissipation rate. This can be seen, for example for the scale to scale energy transfers, dividing equation eq. (2.3) by 4 on both sides such that $\mathcal{E} = \frac{1}{2}(\varepsilon + \varepsilon')$ where $\varepsilon = \nu(\partial u_i/\partial x_k)^2$.

We refer to Marati *et al.* (2004); Danaila *et al.* (2012); Valente & Vassilicos (2015); Alves Portela *et al.* (2017); Mollicone *et al.* (2018); Gatti *et al.* (2020) who give a more detailed interpretation of the various terms in the scale-space framework.

There are several useful observations that follow immediately from deriving the evolution equations for the scale energy, helicity, and enstrophy. These equations resemble their one-point counterparts except that they account for non-linear exchanges across scales through Π. Closer inspection reveals several differences amongst the three budgets. It is clear that transfers of helicity (eq. (2.5)) not only arise from the interactions of the scale to scale helicity δh with the velocity increment δu_k, but also from the interaction of the scale to scale energy δq^2 with the vorticity increment $\delta\omega_k$. This is consistent with the two channels of inter-scale transfer identified in the study of Yan *et al.* (2020) who highlight distinct helicity transfers through the combined action of vortex twisting and vortex stretching arising naturally from the vorticity equation. The pressure term only has an explicit role in the scale energy and helicity budgets. For the scale enstrophy budget, the pressure transport is effectively "curled out", however a non-conservative generation $\mathcal{G}_S$ term emerges whose role is dynamically distinct compared to the pressure transport.

3. Experimental and Numerical Datasets

To exemplify the scale-space framework, two homogeneous turbulence data sets, one experimental and one numerical, are selected. We opt to limit the present scope to homogeneous turbulence for its relative simplicity, but remark that the instantaneous framework is equally applicable to inhomogeneous flows.

3.1. *Von-Kármán Mixing Tank*

The experimental data set considered in this work was gathered in the Göttingen Turbulence Facility #3. The experimental rig consisted of a steel cylinder of diameter and height equal to $48\,cm$ and $58\,cm$ respectively. It featured 8 axial baffles, attached to its inside wall, and two counter-rotating impellers of diameter $25\,cm$ driving the flow inside the cylinder. The rotation frequency was set to $0.2\,Hz$. Water was used as the working fluid (kinematic viscosity of $\nu = 0.98\,mm^2/s$). The flow was seeded with PMMA microspheres with mean diameter $6.0\,\mu m$ and specific gravity $\rho_{\text{seeding}}/\rho = 1.22$ (the resultant particle Stokes number was estimated as $6 \times 10^{-5} \ll 1$). A high-speed Nd:YAG pulse laser was used as the source of illumination. Two high-speed Phantom v640 cameras were used to record the flow. A more in-depth description can be found in Knutsen *et al.* (2020).

The flow inside a cubic domain of $8.5 \times 8.5 \times 8.5\,mm^3$ located at the centre of the tank (where the mean flow vanishes) was measured using scanning Particle Image

Velocimetry (scanning PIV). This measurement technique is extensively discussed in Lawson & Dawson (2014), and here we only include a brief summary of its principles. In the first step, two cameras acquire multiple stereo PIV images, with a very small time separation, as the laser sheet traverses the measurement volume. A volumetric snapshot of the scattered light intensity is subsequently reconstructed from the recorded series of images. Ultimately, cross-correlation of the reconstructed snapshots is performed, yielding a single, volumetric velocity field.

Short, time-resolved sequences of velocity snapshots were captured during the experiment (a correction proposed by Wang *et al.* 2017, was used to reduce the residual divergence of the data). Each sequence consisted of 6 snapshots with the time separation below one-tenth of the Kolmogorov time scale. A vast collection of 2×10^5 such sequences was gathered throughout the experiment. They were considered independent samples of the velocity field as the time separation between sequences was of the order of the impeller revolution period. A Lagrangian filtering, similar to that proposed by Novara & Scarano (2013), was applied to the data in the post-processing phase. Each sequence was used to advect artificial tracers, whose initial positions coincided with the measurement grid points, forward and backwards in time. The resultant traces were utilised to evaluate the filtered velocity and Lagrangian acceleration vectors. The approach described by Lawson & Dawson (2015) was subsequently employed to reconstruct pressure fields. The discretised momentum equation was rearranged to form an over-determined set of linear equations used to solve for pressure in the least-square sense.

The experimental data was stored as cubes containing fields for all components of the velocity, material derivatives, and pressure field (each cube corresponded to one time-resolved measurement sequence). A fourth-order central difference scheme was used to evaluate spatial derivatives.

3.2. *Direct Numerical Simulation*

A DNS data set of forced homogeneous and isotropic turbulence (HIT) provided by the Johns Hopkins University (JHU) turbulence database was used to provide numerical comparison (Li *et al.* 2008). The DNS is triply periodic on a cubic domain of size length 2π with Reynolds number $Re_\lambda = 433$ on a regular grid of 1024^3 points. In time intervals of one second, 256 spatially independent sub-cubes of side length 5λ ($0.4L$) were extracted from the database at full resolution for a total of 2560 sub-cubes over 10 time units (or $5T_L$, where $T_L = u_{rms}/L$ is the large eddy turnover time scale), for which third-order statistics (such as the structure functions reported in section 3.4.2) were found to satisfactorily converge.

The DNS data was stored similarly to the experimental data, where each cube contained fields for all components of the velocity, the material derivatives (accounting for the numerical forcing), and the pressure field. Fourth-order differentiation in physical space was applied directly to the fields as necessary to calculate gradient quantities used in the analysis. As the JHU database enforces the divergence-free condition via spectral methods, a small but non-negligible divergence residual was found for the gradients in physical space. This error was found to propagate to higher-order derivatives; impacting the energy, helicity, and enstrophy budget residuals at approximately 2%, 5%, and 15% respectively (appendix A). Though this error is non-negligible, it is not believed to overshadow the correlation-based conclusions drawn in this study that are primarily rooted in phase information. For the VK data, the error propagation of gradients in physical space is more significant as a result of the limited sub-pixel accuracy. This is discussed in more detail in appendix A, but is particularly problematic for enstrophy

Description	Symbol	VK Tank	JHU DNS
Taylor-microscale Reynolds number	Re_λ	199	433
Normalised grid resolution	$\Delta x/\eta$	0.76	2.2
Normalised temporal resolution	$\Delta t/\tau_\eta$	0.09	0.005
Integral length scale $[mm]$	L	33.7	1.36
Taylor microscale $[mm]$	λ	5.810	0.113
Kolmogorov length scale $[mm]$	η	0.209	0.0028
Kolmogorov time scale $[ms]$	τ_η	45	0.042
Root-mean-square velocity fluctuation $[mm/s]$	u_{rms}	33.6	0.686
Root-mean-square helicity fluctuation $[mm/s^2]$	h_{rms}	838.5	16.67
Root-mean-square vorticity fluctuation $[1/s]$	ω_{rms}	13.12	13.29
Kinetic energy dissipation rate $[mm^2/s^3]$	$\overline{\epsilon^{q^2}}$	492	0.103
Helicity dissipation rate $[mm/s^3]$	$\overline{\epsilon^h}$	9.35	-0.0395
Helicity dissipation rate std. dev. $[mm/s^3]$	ϵ^h_{std}	936	8.88
Enstrophy dissipation rate $[1/s^3]$	$\overline{\epsilon^{\omega^2}}$	2407	1078

Table 1: Parameters from the Von-Kármán Mixing Tank Scanning PIV experiment (Knutsen *et al.* 2020) and the Johns Hopkins University DNS of homogeneous and isotropic turbulence (Li *et al.* 2008). Note the symbols Δx and Δt denote the grid spacing and temporal spacing of the data sets.

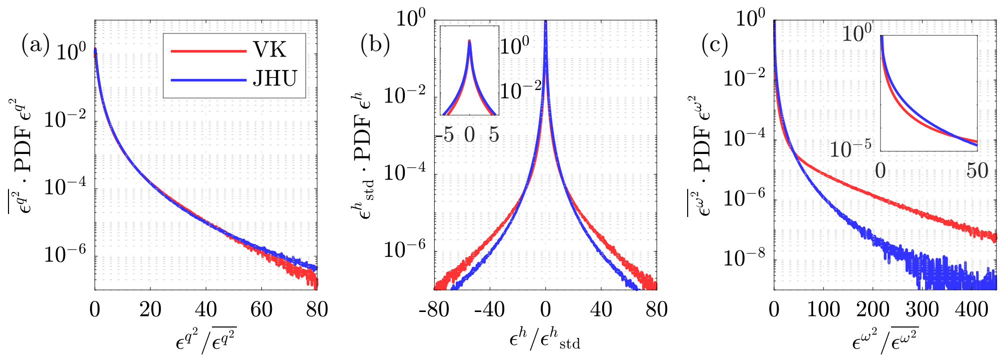

Figure 1: Premulitplied PDFs of the dissipation of energy (a), helicity (b), and enstrophy (c). The inset of (b) highlights the range of helicity dissipation between ±5 standard deviations.

dissipation (fourth order gradients). As a result, conclusions based on such high-order gradients in the VK data are avoided.

3.3. *Characterisation of the data sets*

In this section we characterise the data sets to elucidate the statistical nature of the scale-space energy, helicity, and enstrophy quantities before investigating their transfers in section 4.

The PDFs of the dissipation rates of the energy, helicity, and enstrophy are shown in fig. 1. These distributions are of central importance towards comprehending the scale by scale cascades, as both energy and helicity can only be destroyed by viscous

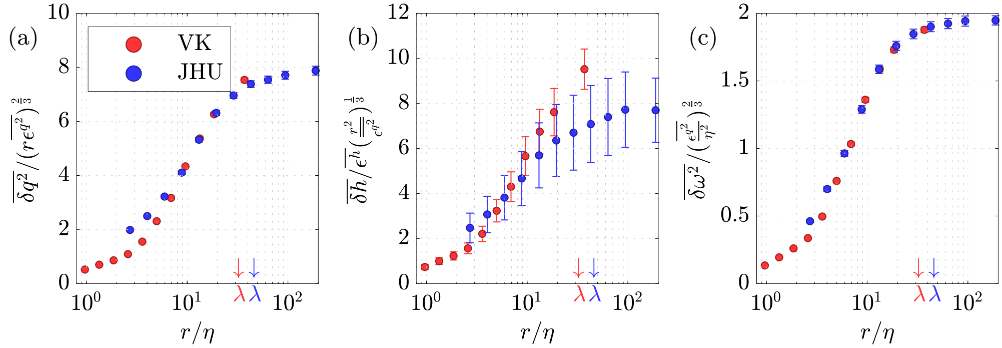

Figure 2: Normalised mean energy structure function $\overline{\delta q^2}$ (a), helicity structure function $\overline{\delta h}$ (b), and enstrophy structure function $\overline{\delta\omega^2}$ (c).

dissipation. The wide tails of these PDFs extend to extreme values resulting in large flatness (Van Atta & Antonia 1980) and are indicative of small-scale intermittency, characteristic of turbulent flows (Sreenivasan & Antonia 1997; Laval *et al.* 2001). The dissipation PDFs agree well between data sets for the energy and helicity, but deviate at extreme values for the dissipation of enstrophy. This is due to the unavoidable PIV error propagation (see appendix A).

3.4. *Ensemble-Averaged Structure functions*

In this section, in addition to the classical energy structure function, the structure functions associated with the helicity and enstrophy are probed; these are central to core theories of turbulence (Zhou 2021). This analysis provides further context on the extension of the scale-space framework beyond that of the scale-space energy budget.

3.4.1. *Energy, Helicity, and Enstrophy Structure Functions*

The energy, helicity, and enstrophy structure functions are presented in fig. 2. Here, and for all scale-space quantities, the overbar denotes both ensemble averaging and averages over all scale-space orientations at a particular scale $r = ||\boldsymbol{r}||$. We note that here (and elsewhere in this study) the error bars correspond to statistical errors obtained using the convergence of the moments of the PDFs (using a 95% confidence interval). Though bias errors arising from experimental artefacts and discretisation are also of concern, they do not dominate the uncertainty. This is supported by the small residual in the energy, helicity, and enstrophy budgets (appendix A).

The energy structure functions in fig. 2(a) are compensated by the classical inertial range scaling $(r\overline{\epsilon^{q^2}})^{2/3}$ (Kolmogorov 1941*a*). The universal constant for the analogous longitudinal second-order structure function is $C_2 \approx 2.0 \pm 0.2$ (Sreenivasan 1995; Pope 2001), however the energy structure functions feature a sum over two transverse components (that scale as $\frac{4}{3}C_2$) and one longitudinal component. Therefore, in the inertial range, the energy structure function is expected to plateau at a value of approximately 7.3 ± 0.7. For the VK data, this value is achieved only at the largest available separation. This is likely due to the limited range of separations, but may also be attributed to the Reynolds number ($Re_\lambda = 199$) for which the inertial range is expected to be limited in breadth (Ishihara *et al.* 2009). For the JHU data the plateau is more evident, however it is also considerably limited due to the sizes of the extracted sub-cubes of side length 5λ.

The helicity structure functions are shown in fig. 2(b). As the helicity is not a sign-definite quantity, the structure functions were found to converge very slowly due to their characteristically high variation (Kurien *et al.* 2004). The helicity structure functions are normalised using the inertial range scaling in physical space as $\overline{\delta h}/\overline{\epsilon^h}(r^2/\overline{\epsilon^{q^2}})^{1/3}$ outlined by Brissaud *et al.* (1973). A developing plateau is observed for the JHU data for $r > \lambda$ in agreement with the energy structure function. Also consistent with its energy structure function and limited range of separations, the VK data does not show a clear plateau for $\overline{\delta h}$. The overlap within uncertainty between the two data sets indicates satisfactory collapse, though curiously this occurs mostly for r in the near-dissipative range. The lack of large separations r in the VK data prevents from evaluating the collapse of the data sets for $r > \lambda$ (in the inertial range).

Despite the lack of explicit helical forcing in the DNS, the scale-space helicity is non-zero for both data sets. This is consistent with the helicity spectrum computed over a wide range of simulations (Chen *et al.* 2003; Mininni *et al.* 2006) with and without helical forcing (Alexakis 2017). This can be seen directly through an expansion of $\overline{\delta h}$, i.e. for homogeneous turbulence $\overline{(u_i - u_i')(\omega_i - \omega_i')} = 2\overline{h} - 2\overline{u_i\omega_i'}$. This reveals that even when small-scale mirror symmetry holds ($\overline{h} = 0$) the non-zero scale space helicity (and spectrum of helicity) arises from the coherence in the velocity-vorticity correlation (Levich & Shtilman 1988). This was shown explicitly for isotropic turbulence by Deusebio *et al.* (2014). The present results confirm this non-zero correlation as well as the tendency of the turbulence cascade to restore small-scale mirror symmetry with decreasing scale (Kraichnan 1973; Chen *et al.* 2003).

The enstrophy structure functions are presented in fig. 2(c) normalised using the energy dissipation rate and the Kolmogorov length scale $\eta = (\nu^3/\overline{\epsilon^{q^2}})^{1/4}$ as $(\overline{\epsilon^{q^2}}/\eta^2)^{2/3}$. A normalization using $\overline{\epsilon^{\omega^2}}$ was tested but found to give unsatisfactory agreement (likely due to error propagation, see Appendix A). The close relationship between the enstrophy and the dissipative small scales (Jiménez *et al.* 1993) implies a constant scaling in the inertial range. Consistent with the energy and helicity structure functions, the enstrophy structure functions reach a maximum only for the largest separations and more conclusively for the JHU data. This reaffirms enstrophy as quantity that is confined to the small scales (Jiménez *et al.* 1993; Davidson *et al.* 2008; Ishihara *et al.* 2013; Elsinga *et al.* 2017).

3.4.2. *Non-linear Flux Energy, Helicity, and Enstrophy Structure Functions*

In this section the non-linear flux (NLF) structure functions, of which the divergence is taken in the non-linear inter-scale transfers Π, are explored. A small departure to justify this terminology will be taken here. These structure functions are commonly referred to as "third-order structure functions", but as the origin of "third order" is in the statistical moment of the increment of a single quantity (i.e. $\overline{\delta u^3}$) a different terminology is adopted for improved generality. As noted by Hill (2002), making use of Gauss' theorem when integrating the non-linear energy transfer term of eq. (2.3) inside a ball $\mathcal{V}_R$ (defined in the space of scales as $\{\boldsymbol{r} \in \mathbb{R}^3 : |\boldsymbol{r}| \leqslant R\}$) gives $\iiint \Pi^{q^2} \,\mathrm{d}\mathcal{V}_R = \oiint_{\partial\mathcal{V}_R} \overline{\delta u_k \delta q^2} n_k \,\mathrm{d}\mathcal{S}$ with n_k the outward normal vector and $d\mathcal{S}$ the surface of the spherical shell (the boundary of $\mathcal{V}_R$). The orientation average over the spherical shell is identically zero, leaving only a flux in the radial direction. This motivates referring to these quantities as non-linear flux (NLF) structure functions in the present context. In addition to the central role of NLF structure functions in classical turbulence theory, i.e. the 4/5ths (K41) and 2/15ths laws (Chkhetiani 1996; L'vov *et al.* 1997), their physical significance is well documented in the context of a spherical scale-space coordinate system (Valente & Vassilicos 2015;

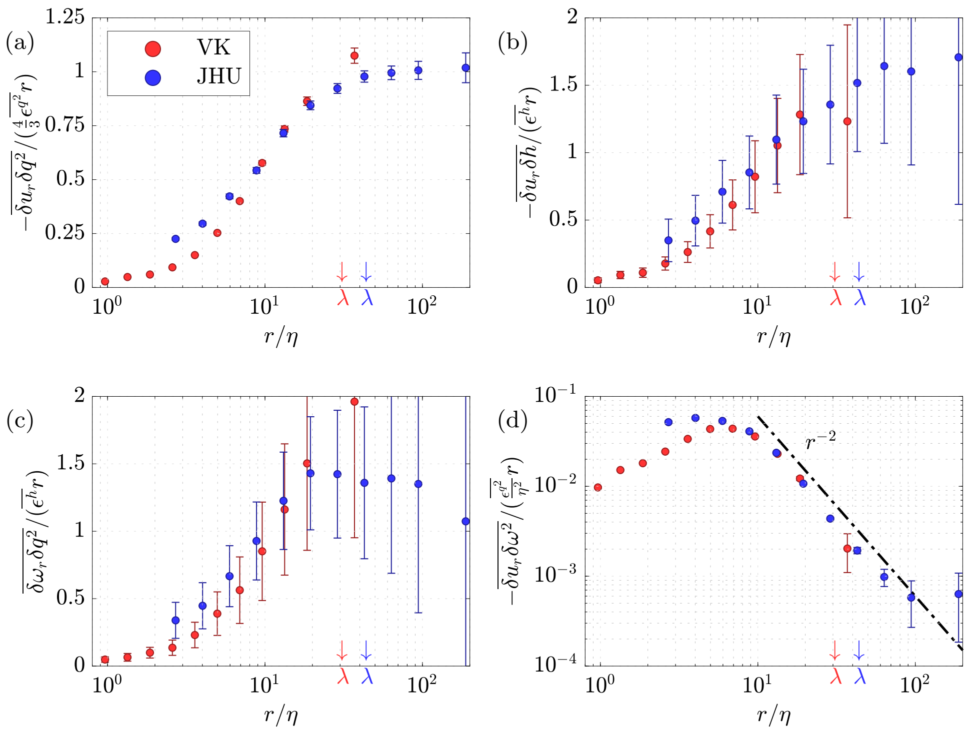

Figure 3: Normalised orientation-averaged NLF structure functions corresponding to the non-linear scale-to-scale flux of energy $\overline{\delta q^2}$ (a), helicity $\overline{\delta h}$ via advection (b) and vortex stretching (c), and enstrophy $\overline{\delta \omega^2}$ (d).

Gomes-Fernandes *et al.* 2015; Alves Portela *et al.* 2017). The NLF structure functions for the experimental and numerical data sets are presented in fig. 3.

The orientation-averaged NLF energy structure function is shown in fig. 3(a) normalised using the classical 4/3rds law (Hill 2002). The subscript "r" is used to denote the radial flux as described above. For $r > \lambda$ the plateau seen in the JHU data suggests classical behavior of $\overline{\delta u_r \delta q^2}$. Consistent with fig. 2, the VK data does not show a clear plateau developing for $\overline{\delta u_r \delta q^2}/\frac{4}{3}\overline{\varepsilon^{q^2}}r$, but does reach value close to one at $r \approx \lambda$ (the largest available separation). This may imply the non-linear inter-scale transfer is dominant at $r = \lambda$ (Yasuda & Vassilicos 2018), but it must be noted that such an apparent balance is possible when some inhomogeneous effects are at play (Alves Portela *et al.* 2017).

The orientation-averaged NLF helicity structure functions are shown in figures 3(b) and 3(c) normalised using the product of r and dissipation rate of helicity $\overline{\epsilon^h}$. This normalisation is chosen to compare the two distinct mechanisms associated with $\overline{\Pi^h}$ in eq. (2.5). The first, $\overline{\delta u_k \delta h}$, originates from the advective term and the second, $\overline{\delta \omega_k \delta q^2}$, from the vortex stretching term of eq. (2.2) (Yan *et al.* 2020). It is again seen that, due to its non-positive definiteness and inherently high variation, the non-linear flux of helicity is very slow to converge, leading to large uncertainty bars. Despite this, they are found to be non-zero and the JHU data appears to exhibit a plateau (albeit within large uncertainty bars).

Finally, the normalised NLF enstrophy structure functions can be seen in fig. 3(d).

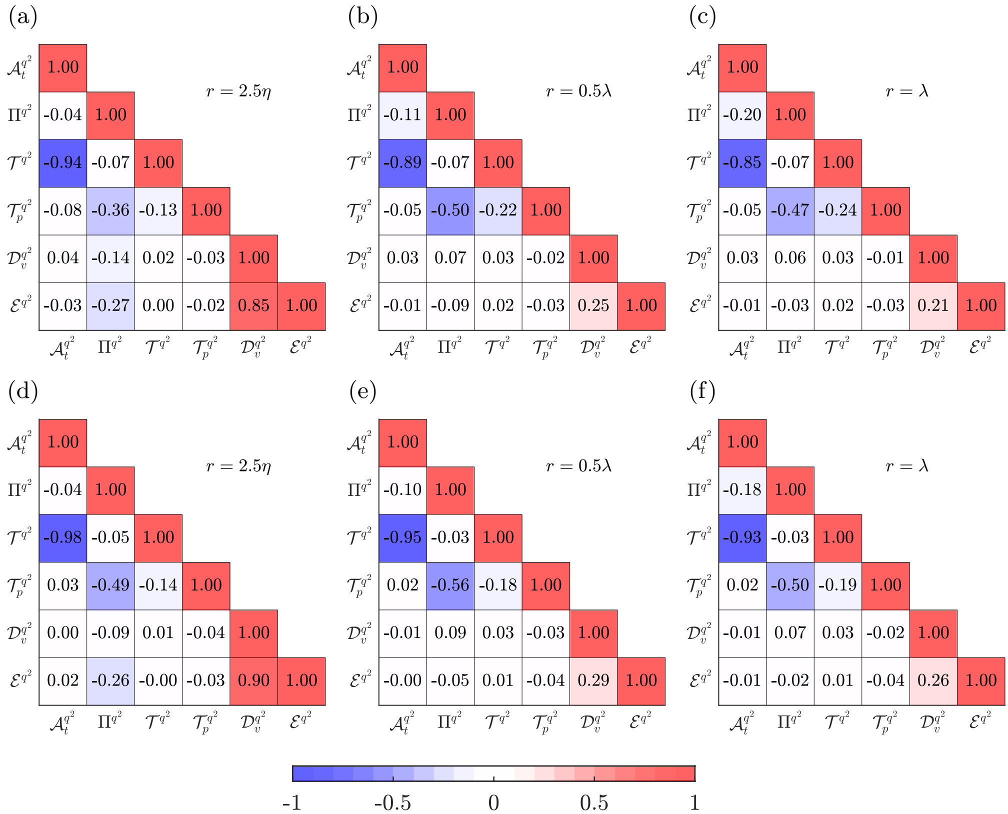

Figure 4: Correlation coefficients between terms of eq. (2.4) for δq^2 at various separations; results based on VK (a)-(c) and JHU (d)-(f) datasets.

Similarly to the enstrophy structure function, a collapse of the data sets is observed in the near-dissipation range between $r/\eta = 10$ and $r/\lambda = 1$. The flux is seen to decrease as r^{-3} (r^{-2} in the figure due to compensating $-\overline{\delta u_r \delta \omega^2}$ by r) into the inertial range. This power law decrease is consistent with the results of Davidson *et al.* (2008) (in their case, a scale-by-scale enstrophy flux is defined that is not motivated by the present spherical scale-space coordinate system. This necessitates compensating $-\overline{\delta u_r \delta \omega^2}$ by r for a one-to-one comparison).

4. Correlations of Instantaneous Cascades

4.1. *Correlations within budgets*

Normalised correlations (-1: perfectly anti-correlated, 0: uncorrelated, and 1: perfectly correlated) were tabulated as outlined in appendix A. We shall focus on the separations $r = 2.5\eta$, 0.5λ, and λ that correspond to the dissipative and near-dissipative ranges, and the onset of inertial range, respectively. The latter is of particular interest, as it is the scale for which Yasuda & Vassilicos (2018) identified the largest variations in energy transfers (standard deviation) in periodic box turbulence with $Re_\lambda = 178$, indicative of strong dynamics at that scale.

The correlations of the terms in the scale energy, helicity, and enstrophy budgets are presented in figures 4, 5, and 7, respectively. Starting with the energy in figure 4, the correlations of terms are in good agreement across the three considered scales between both the JHU and VK data. At the smallest r, the high correlation between the viscous diffusion and dissipation seen in fig. 4(a) and 4(d) reflects the average balance between $\mathcal{D}_\nu^{q^2}$ and $\mathcal{E}^{q^2}$, as noted by (Valente & Vassilicos 2015).

The most robust correlation of figure 4 lies between the unsteady transport $\mathcal{A}_t^{q^2}$ and the turbulent transport $\mathcal{T}^{q^2}$. This is taken to be the signature of the random sweeping effect identified by Yasuda & Vassilicos (2018), who found that random sweeping indeed extends from single- to two-point quantities. (Strictly speaking, the random sweeping effect is reflected in the correlation between $\mathcal{A}_t^{q^2}$ and $(\mathcal{T}^{q^2} - \Pi^{q^2})$. However, in the present analysis, we restrict to correlations between individual terms, but remark that the signature of random sweeping is consistent with the results of Yasuda & Vassilicos (2018).) As $\mathcal{T}$ is associated with transport in physical space, its high correlation with $\mathcal{A}_t^{q^2}$ is likely a result of the known preferential anti-alignment between the unsteady acceleration $\frac{\partial}{\partial t} u_i$ and the convective acceleration $u_k \frac{\partial}{\partial x_k} u_i$ (Tsinober 2001).

Turning attention to the non-linear transfer Π^{q^2}, an anti-correlation with the pressure transport term $\mathcal{T}_p^{q^2}$ is seen to persist across all scales investigated here. As the pressure (and resulting pressure transport) results from a volumetric integration of the velocity field over the entire flow domain, the non-local influence of the baffles of the VK tank and the numerical forcing of the JHU data could non-trivially impact the role of the pressure transport. Despite this, a significant anti-correlation between $\mathcal{T}_p^{q^2}$ and Π^{q^2} persists between both data sets, indicating a dynamical link between those quantities.

As seen in fig. 5, the correlations between the terms involved in the scale to scale helicity budget show some similarities with those observed for the energy budget. At the smallest scales, the same positive correlation between $\mathcal{D}_\nu^h$ and $\mathcal{E}^h$ is seen just as in the energy, reflecting the destruction of helicity by viscous forces. The signature of the random sweeping effect is again identified from the correlation between $\mathcal{A}_t^h$ and $\mathcal{T}^h$ at all r. In contrast to the energy transfers, however, the pressure transport $\mathcal{T}_p^h$ appears to have an increasing correlation with the non-linear transfer Π^h as r decreases.

Before this result is discussed for the helicity cascade in more depth, it is necessary to adopt the framework presented by Yasuda & Vassilicos (2018) for the energy budget. As in their work, the correlation of $\mathcal{T}_p^{q^2}$ and $|\delta \boldsymbol{u}||\delta \nabla p|$ is confirmed to be negligible in the present study. On the other hand, defining the cosine of the angle between $\delta \boldsymbol{u}$ and $-\delta \boldsymbol{\nabla} p$ as

$$\cos\phi_u = (\widehat{\delta \boldsymbol{u}} \cdot \hat{\boldsymbol{r}})(-\widehat{\delta \nabla p} \cdot \hat{\boldsymbol{r}}) + (\widehat{\delta \boldsymbol{u}} \times \hat{\boldsymbol{r}}) \cdot (-\widehat{\delta \nabla p} \times \hat{\boldsymbol{r}}) \tag{4.1}$$

where $\hat{\cdot}$ denotes unit norm, we find that the correlation of $\mathcal{T}_p^{q^2}$ with $\cos\phi_u$ is substantial. This is shown in fig. 6(a) for the JHU data but similar results were found for the VK data (these are omitted for brevity).

From both the dot product and cross product contributions of eq. (4.1), Yasuda & Vassilicos (2018) found that the mean was small but positive. This implies that in the averaged picture the convergence events (i.e. $\delta \boldsymbol{u} \cdot \hat{\boldsymbol{r}} < 0$) occur simultaneously with compressing forces (i.e. $-\widehat{\delta \nabla p} \cdot \hat{\boldsymbol{r}} < 0$), and vice-versa, divergence events are coupled to expanding pressure forces. Importantly, one may conclude based on the identity between the (scale-space) volume integral $\iiint_{\mathcal{V}_R} \Pi^{q^2} \,\mathrm{d}\mathcal{V}_R$ and surface integral $\oiint_{\partial \mathcal{V}_R} \delta \boldsymbol{u} \cdot \hat{\boldsymbol{r}} \delta q^2 \,\mathrm{d}\mathcal{S}$ that the convergence events facilitate the forward δq^2 cascade, whereas divergence events facilitate the inverse cascade (Yasuda & Vassilicos 2018). And further, it can be inferred

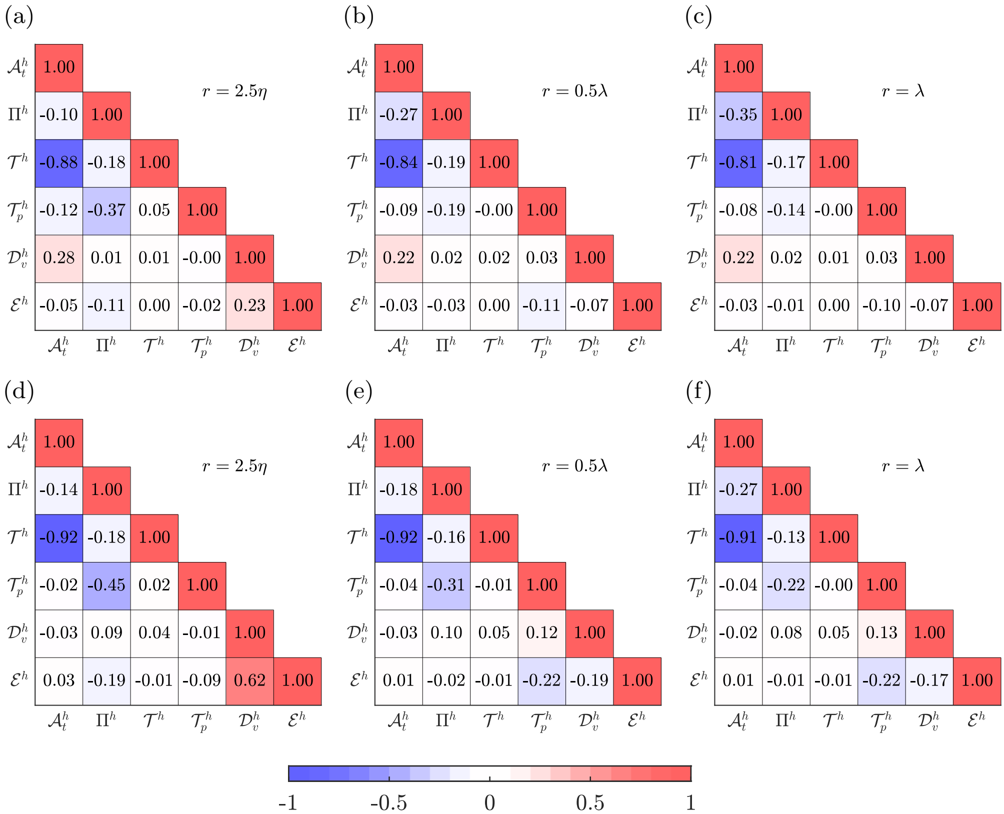

Figure 5: Correlation coefficients between terms of eq. (2.6) for δh at various separations; results based on VK (a)-(c) and JHU (d)-(f) datasets.

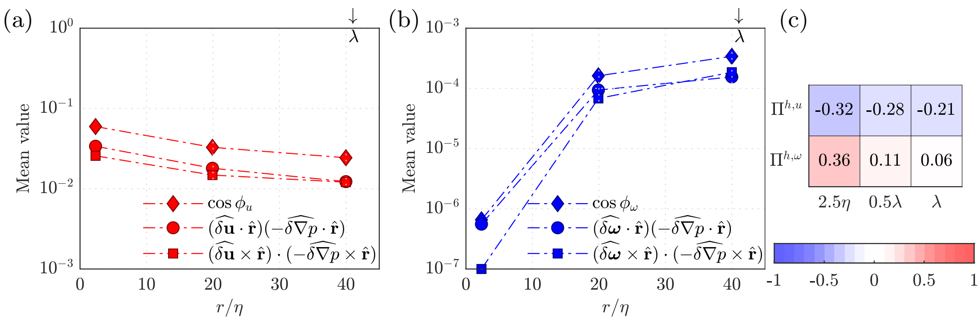

Figure 6: Mean value of the alignment between unit vectors of the velocity (a) and vorticity (b) increments via (eqns 4.1 and 4.2). The correlations of the non-linear helicity transfer mechanisms $\Pi^{h,u}$ and $\Pi^{h,\omega}$ (see text for definitions) with the pressure transport of helicity $\mathcal{T}_p^h$ are shown in (c). All results are from the JHU data.

from the positive value of mean $\cos\phi_u$ that the forward cascading of δq^2 coincides also with compressing forces.

Returning to the correlation of Π^h with $\mathcal{T}_p^h$ in the present study, it is apparent that the role of the pressure transport is comparatively more complex. This is because Π^h features two distinct NLF structure functions arising from the vortex twisting and stretching mechanisms (Yan *et al.* 2020). The mechanisms are separated here such that $\Pi^h = \Pi^{h,u} - \Pi^{h,\omega}$ where $\Pi^{h,u} = \frac{\partial}{\partial r_k}\delta u_k \delta h$ (vortex twisting) and $\Pi^{h,\omega} = \frac{1}{2}\frac{\partial}{\partial r_k}\delta\omega_k \delta q^2$ (vortex stretching). As a near-zero correlation of $\mathcal{T}_p^h$ with $|\delta\boldsymbol{\omega}||\delta\nabla p|$ was found, an analogous analysis to Yasuda & Vassilicos (2018) may be attempted using the angle defined via

$$\cos\phi_\omega = (\widehat{\delta\boldsymbol{\omega}}\cdot\hat{\boldsymbol{r}})(-\widehat{\delta\nabla p}\cdot\hat{\boldsymbol{r}}) + (\widehat{\delta\boldsymbol{\omega}}\times\hat{\boldsymbol{r}})\cdot(-\widehat{\delta\nabla p}\times\hat{\boldsymbol{r}}). \tag{4.2}$$

The alignment for both the dot product and cross product contributions were similarly found to be small but positive as can be seen in fig. 6(b). The meaning of this alignment, however, is not trivial in the case of helicity. Such a correlation is expected to vanish in mirror-symmetric flow for lack of a preference for any specific sense of rotation (imposed by the sign of $\widehat{\delta\boldsymbol{\omega}}\cdot\hat{\boldsymbol{r}}$). The non-zero average of $\cos\phi_\omega$, increasing with r, is reminiscent of the scale-to-scale helicity itself (fig. 2(b)).

To reconcile the meaning of this result, we shall clarify the direction of the helicity cascade in the following. In contrast to δq^2, the terms “forward cascade” and “inverse cascade” are not well-established in the context of helicity (Alexakis 2017), due to the lack of positive definiteness of δh. To address this, an auxiliary quantity H_R is introduced as a reference for the sense of rotation as

$$H_R = \iiint_{\mathcal{V}_R} \underbrace{(\delta\boldsymbol{u}\cdot\hat{\boldsymbol{r}})(\delta\boldsymbol{\omega}\cdot\hat{\boldsymbol{r}})}_{\delta h_R}\,\mathrm{d}\mathcal{V}_R. \tag{4.3}$$

The forward and backward directions of the helicity cascade is then defined based on the sign of H_R (i.e. $\frac{H_R}{|H_R|}$). The helicity cascading events causing $\frac{H_R}{|H_R|}\iiint_{\mathcal{V}_R}\Pi^h\,\mathrm{d}\mathcal{V}_R < 0$ are deemed to cascade forward, while $\frac{H_R}{|H_R|}\iiint_{\mathcal{V}_R}\Pi^h\,\mathrm{d}\mathcal{V}_R > 0$ implies inverse cascading. Similarly to δq^2, analogous relations invoking the divergence theorem may be drawn for the non-linear transfer terms: $\iiint_{\mathcal{V}_R}\Pi^{h,u}\,\mathrm{d}\mathcal{V}_R = \oiint_{\partial\mathcal{V}_R}\delta\boldsymbol{u}\cdot\hat{\boldsymbol{r}}\delta h\,\mathrm{d}\mathcal{S}$ and $\iiint_{\mathcal{V}_R}\Pi^{h,\omega}\,\mathrm{d}\mathcal{V}_R = \frac{1}{2}\oiint_{\partial\mathcal{V}_R}\delta\boldsymbol{\omega}\cdot\hat{\boldsymbol{r}}\delta q^2\,\mathrm{d}\mathcal{S}$. It follows that events of $\frac{\delta h H_R}{|\delta h||H_R|}\delta\boldsymbol{u}\cdot\hat{\boldsymbol{r}} < 0$ and $\frac{H_R}{|H_R|}\delta\boldsymbol{\omega}\cdot\hat{\boldsymbol{r}} > 0$ facilitate the forward helicity cascade and vice-versa for the inverse cascade.

It is important to note that the two mechanisms (i.e. stretching and twisting) cascade helicity in the same direction (either upscale or downscale) only when $\delta h\delta h_r < 0$. Additionally, a positive mean value of $\cos\phi_\omega$ (as in fig. 6(b)) suggests that when the signs of H_R and $\delta\boldsymbol{\omega}\cdot\hat{\boldsymbol{r}}$ are in agreement, the downscale helicity cascade couples with expanding pressure forces and the upscale helicity cascade associates with compressing pressure forces (in the averaged sense).

The correlations of the individual vortex twisting and stretching mechanisms with $\mathcal{T}_p^h$ in fig. 6(c) shows a clear distinction between mechanisms. In the former, the correlation is relatively steady within the probed separation range, similar to what is seen in the context of δq^2. On the other hand, the stretching mechanism exhibits strong interactions with pressure forces (stronger than the twisting) at dissipative scales, which diminish almost entirely by the time r reaches λ.

Finally, we turn out attention to the correlations of the transfer terms of the scale to scale enstrophy are presented in fig. 7. As explained in Appendix A, noise propagation in the VK data renders correlations of $\mathcal{A}_t^{\omega^2}$ and $\mathcal{E}^{\omega^2}$ particularly erroneous. The results of the VK data are therefore omitted.

A striking similarity with the energy and helicity budgets is immediately apparent through the anti-correlation of the unsteady transport $\mathcal{A}_t^{\omega^2}$ and turbulent transport $\mathcal{T}^{\omega^2}$. This confirms the random sweeping effect persists across all budgets and across all

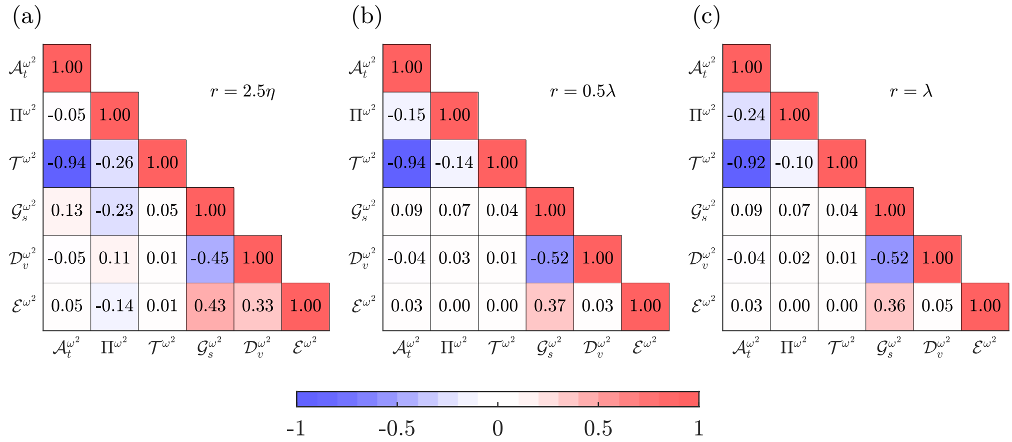

Figure 7: Correlation coefficients between terms of eq. (2.8) for $\delta\omega^2$ at various separations of JHU data (a)-(c).

scales. The generation term $\mathcal{G}_s^{\omega^2}$ exhibits a positive correlation with $\mathcal{E}^{\omega^2}$ and a negative correlation with $\mathcal{D}_\nu^{\omega^2}$. This implies a concurrent enstrophy generation and dissipation mechanism (Davidson *et al.* 2008). This simultaneous generation and dissipation is tied to a reduction (during high dissipative events) or increase (during low dissipative events) in the diffusion of enstrophy. This is seen to persist across all scales considered. A small positive correlation between $\mathcal{D}_\nu^{\omega^2}$ and $\mathcal{E}^{\omega^2}$, akin to the energy and helicity cascades, is seen only for $r = 2.5\eta$.

4.2. *Correlations between budgets*

We now explore possible connections between budget equations, i.e. correlations between the mechanisms involved in the budget of a given scale-by-scale structure function and those of the others, as shown in fig. 8. The correlations between both the scale energy and enstrophy transfers and the helicity transfers were found to be universally of order 10^{-2} and are thus omitted. At first glance, this appears to contradict a wealth of research that has identified clear causal relationships between the three quantities (Bershadskii *et al.* 1994; Biferale *et al.* 2013; Alexakis 2017; Bos 2021) even analytically (via Lagrangian closure theory, see Inagaki 2021). As discussed by Tsinober (2001), near-zero correlations are necessary, but not sufficient, to determine that two quantities are unrelated. For example, the unsteady term $\frac{\partial u_i}{\partial t}$ (eq. (2.1)) is almost entirely decorrelated with the material acceleration $\frac{Du_i}{Dt}$ simply due to the underlying anti-correlation of $\frac{\partial u_i}{\partial t}$ with $u_k \frac{\partial u_i}{\partial x_k}$.

In the present case, the root of the decorrelation is likely to be the fact that helicity is not positive-definite (Kurien *et al.* 2004). Alternatively, a geometric approach allows to separate the transfer quantities into the product of a (positive-definite) norm with an appropriately defined angle (Yasuda & Vassilicos 2018). This avenue for further insight is explored in section 5.

Let us now return to fig. 8, which shows correlations between energy and enstrophy budgets. The most robust correlation is that between dissipation rate of energy $\mathcal{E}^{q^2}$ and the dissipation rate of enstrophy $\mathcal{E}^{\omega^2}$, with a magnitude exceeding 0.5 across all considered scales. Figure 8 also shows that the energy dissipation $\mathcal{E}^{q^2}$ and enstrophy diffusion $\mathcal{D}_\nu^{\omega^2}$ are negatively correlated whereas the energy dissipation $\mathcal{E}^{q^2}$ and enstrophy

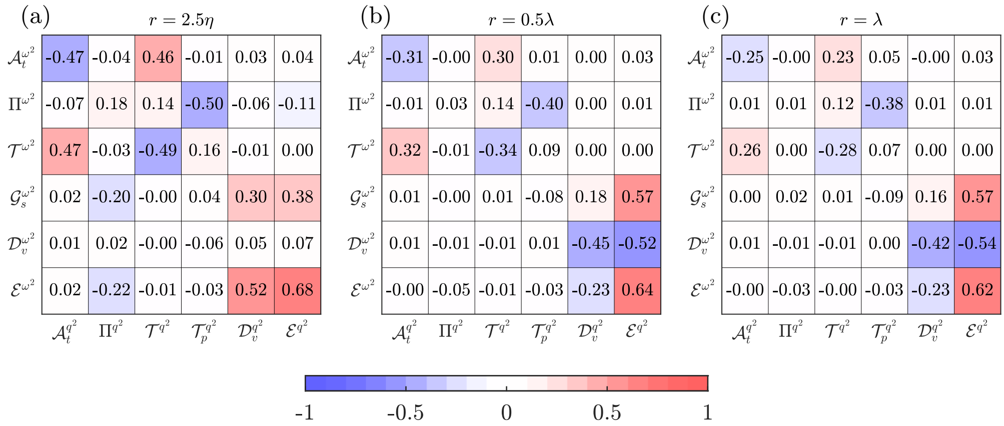

Figure 8: Correlation coefficients between terms of eqs. (2.4) and (2.8) (respectively transfers terms of δq^2 and $\delta\omega^2$ on the horizontal and vertical axis) at various separations of JHU data (a)-(c).

generation $\mathcal{G}_s^{\omega^2}$ (for $r = 0.5\lambda$ and $r = \lambda$) are positively correlated. Together, these observations support the classical picture that the generation of scale enstrophy at the small-scales (Siggia 1981) is largely responsible for the dissipation of energy (as well as enstrophy generation, Siggia 1981). Finally, the signature of the random sweeping effect can be clearly seen amongst the correlations between $\mathcal{A}_t$ and $\mathcal{T}$ in fig. 8, particularly at the smallest scales. Together, these mechanisms point to the interconnected nature of the simultaneous turbulence exchanges.

5. Influence of Scale-Space Helicity on the Energy Cascade

5.1. *Application of Lamb Decomposition*

In the previous section, it was found that the correlation between transfers of energy and transfers of helicity was zero. There is however evidence that the magnitude of the helicity itself has an impact on the local transfer of energy. Regions of high helicity are thought to suppress non-linear energy transfer and dissipation (Pelz *et al.* 1985; Stepanov *et al.* 2015), though some results suggest otherwise (Zhou *et al.* 2016). To probe more closely the connection between the helicity and the energy cascade in the present study, the Lamb decomposition is invoked on the non-linear term of eq. (2.1):

$$u_k \frac{\partial}{\partial x_k} u_i = \frac{1}{2} \frac{\partial}{\partial x_i}(u_k u_k) + \epsilon_{jki}\omega_j u_k \tag{5.1}$$

where $\epsilon_{jki}\omega_j u_k = \boldsymbol{\omega} \times \boldsymbol{u}$ is known as the Lamb vector. This quantity is central to the non-linear turbulence cascade as maximal helicity $h = \boldsymbol{\omega} \cdot \boldsymbol{u}$, i.e. the alignment of $\boldsymbol{u}$ and $\boldsymbol{\omega}$, corresponds to a suppression of non-linearity $\boldsymbol{\omega} \times \boldsymbol{u}$ in the Navier-Stokes equation.

A kinematic connection can be gleaned from eq. (2.1) invoking eq. (5.1). Similarly to the derivation of the KHMH energy (section 2) but focusing on the non-linear terms exclusively, it follows that

$$
\begin{aligned}
2\delta u_i(u_k\frac{\partial}{\partial x_k}u_i - u'_k\frac{\partial}{\partial x'_k}u'_i) = -2\varSigma u_k\epsilon_{jik}\delta\omega_j\delta u_i \\
+\frac{\partial}{\partial r_k}(\delta q^2\delta u_k) - \frac{1}{2}\frac{\partial}{\partial X_k}(\varSigma u_k\delta q^2) + 2\frac{\partial}{\partial r_i}(\delta u_i\varSigma q^2).
\end{aligned}
\tag{5.2}
$$

After simplification, this leads to the triple product relation

$$
\varSigma \boldsymbol{u}\cdot(\delta\boldsymbol{\omega}\times\delta\boldsymbol{u}) = \varPi^{q^2>} - \mathcal{T}^{q^2<}
\tag{5.3}
$$

where $\varPi^{q^2>} = \frac{\partial}{\partial r_i}(\delta u_i\varSigma q^2)$ is the non-linear scale-to-scale transfer for the energy sum $\varSigma q^2 = \varSigma u_i\varSigma u_i$ and $\mathcal{T}^{q^2<} = \frac{1}{2}\frac{\partial}{\partial X_k}(\varSigma u_k\delta q^2)$ is the usual non-linear energy transport from eq. (2.4). Hereafter the superscripts $<$ and $>$ are used for shorthand to refer to transfer of the increment and the sum quantities, respectively. A detailed derivation of this result is provided in appendix B.

An immediate curiosity stems from the presence of the energy sum non-linear transfer $\varPi^{q^2>}$. The dynamical significance of the energy (or velocity) sum is a matter of some debate, but has been linked to so-called "large-scale intermittency" in previous studies (Sreenivasan & Antonia 1997; Blum *et al.* 2010; Chien *et al.* 2013; Carter & Coletti 2018). To summarize, instances when the energy sum is large and within the range of correlated scales (large-scale sweeping motions) have been shown to increase the content of the energy structure functions relative to the mean at each scale. This implies a connection between large and small scales in turbulence (Mininni *et al.* 2006; Hosokawa 2007). eq. (5.3) indicates these sweeping motions play a central role in non-linear energy transport. It shows that sufficiently large $\varSigma\boldsymbol{u}$ can overcome the alignment of $\delta\boldsymbol{u}$ and $\delta\boldsymbol{\omega}$ (as long as they not perfectly aligned). This could explain some conflicting results where strong dissipation is found even when these quantities are aligned and helicity is maximal (Zhou *et al.* 2016).

Particularly for turbulence theory, the kinematic connection revealed by eq. (5.2) provides novel insight into the mechanics of the energy cascade. By substituting for $\mathcal{T}^{q^2<}$ in eq. (2.4) using eq. (5.2) and invoking steady, homogeneous turbulence within an independent intermediate range of scales (Kolmogorov 1941*a*,*b*), it is found upon ensemble averaging that

$$
\overline{\varSigma \boldsymbol{u}\cdot(\delta\boldsymbol{\omega}\times\delta\boldsymbol{u})} = 4\overline{\epsilon^{q^2}}.
\tag{5.4}
$$

By virtue of homogeneity, the sum $\overline{\varPi^{q^2>}} + \overline{\varPi^{q^2<}} = 0$ and therefore no longer features in the balance with the dissipation rate of energy. This can be shown analytically and was verified for both data sets in the present study (not shown for brevity). This demonstrates the high relevance of the triple product on the LHS of eq. (5.4). It is not only a feature of the instantaneous kinematics, but also central to the overall dynamics. It is perhaps unwelcome to see the velocity sum play a central role in the mean rate of energy dissipation in the inertial range, as this challenges the possibility that there exists a range of scales independent of the large-scale effects (or of the forcing). Such an observation has been previously identified in terms of triadic interactions (Yeung & Brasseur 1991), but to the authors knowledge this is the first such demonstration in real space. This provides direct insight on the role of large-scale intermittency (via $\varSigma\boldsymbol{u}$) on the inertial range in the cascade of energy (Sreenivasan & Antonia 1997).

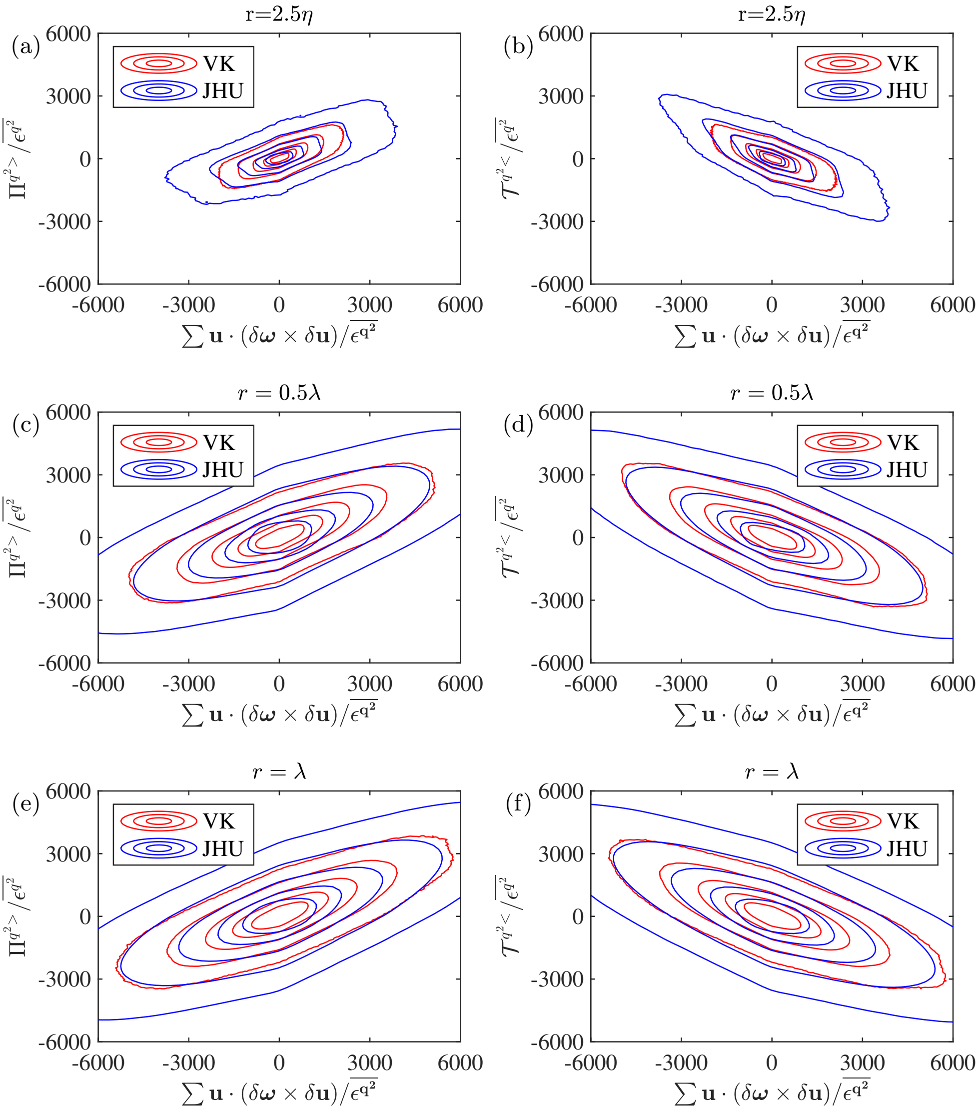

Figure 9: Joint PDFs of the triple product of eq. (5.3) with the non-linear energy sum transfer $\Pi^{q^2>}$ (a,c,e) and non-linear energy transport $\mathcal{T}^{q^2<}$ (b,d,f) for $r = 2.5\eta$ (a,b), $r = 0.5\lambda$ (c,d) and $r = \lambda$ (e,f). Contour values range from 10^{-12} to 10^{-8} (counting from the outermost line).

Equation (5.4) highlights a geometric perspective of the energy dissipation, where the mean projection of the velocity sum onto the cross product of the velocity and vorticity increment balances the mean dissipation rate. By virtue of the fact that $||\delta\boldsymbol{u}\times\delta\boldsymbol{\omega}||^2 = ||\delta\boldsymbol{u}||^2||\delta\boldsymbol{\omega}||^2 - ||\delta h||^2$, there is an implicit connection between the dissipation of energy and the scale-by-scale helicity. Although this does not necessarily connect the transfers, or dynamics, of the two quantities together it does show that the magnitude of the scale-space helicity influences the dissipation of energy (but also, critically, depends on the alignment with sweeping motions).

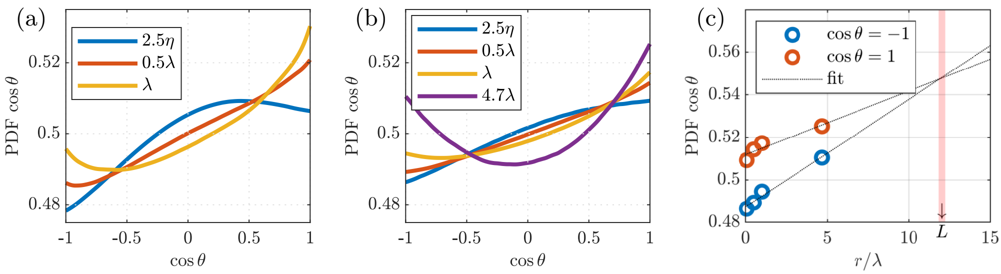

Figure 10: PDF of $\cos\theta$ characterising the alignment between the velocity sum and the cross product (eq. (5.3)) for the VK data (a) and JHU data (b), and an extrapolation of the PDF at extreme values of $\cos\theta$ for JHU data (c) (L marks the integral length scale).

Having identified the statistical significance of the triple product, we turn our attention to the instantaneous behaviour. Motivated by the kinematics of eq. (5.3), the joint PDFs of the triple product with the non-linear energy sum transfer $\Pi^{q^2>}$ and the non-linear energy transport $\mathcal{T}^{q^2<}$ were computed for the VK and JHU data sets and plotted in fig. 9. There is a clear positive and negative correlation between the triple product and $\Pi^{q^2>}$ and $\mathcal{T}^{q^2<}$, respectively, with very close agreement in terms of the slope (± 0.5) of the major axis of the ellipse formed by the joint PDFs. In fact, eq. (5.2) requires the slopes be complementary. The slope, and therefore the underlying correlation, is robust across all scales considered and for both the experimental and numerical data sets. The increase in intermittency (i.e. the flatness of the joint PDFs) with increasing scale is reminiscent of large-scale intermittency (Sreenivasan & Antonia 1997).

It is of interest that the triple product reveals a similar correlation to both $\Pi^{q^2>}$ and $\mathcal{T}^{q^2<}$ separately. This originates with the velocity sum $\Sigma\boldsymbol{u}$, featuring both in the triple product and via $\mathcal{T}^{q^2<} = \Sigma\boldsymbol{u}\cdot\frac{\partial}{\partial \boldsymbol{X}}(\frac{\delta q^2}{2})$. This establishes an immediate and scale-independent connection between the two quantities. The remaining correlation between the triple product and $\Pi^{q^2>}$ follows as a direct consequence of eq. (5.3). Despite their closely tied kinematics, there are important dynamic distinctions amongst the quantities involved in terms of their statistical behaviour. Under the assumption of homogeneity, the ensemble average $\overline{\mathcal{T}^{q^2<}} = 0$ whereas $\overline{\Pi^{q^2>}} = -\overline{\Pi^{q^2<}}$, and $\overline{\Sigma\boldsymbol{u}\cdot(\delta\boldsymbol{\omega}\times\delta\boldsymbol{u})} = 4\overline{\epsilon^{q^2}}$. This motivates the interpretation of $\Pi^{q^2>}$ as a transfer of energy to larger scales whose average is a complement to $\overline{\Pi^{q^2<}}$.

The establishment of an overall balance between the triple product and the dissipation of energy in the inertial range (eq. (5.4)) motivates further insight into the alignment of $\Sigma\boldsymbol{u}$ and $(\delta\boldsymbol{\omega}\times\delta\boldsymbol{u})$. This is quantified using the angle defined by

$$\cos\theta = \frac{\Sigma\boldsymbol{u}\cdot(\delta\boldsymbol{\omega}\times\delta\boldsymbol{u})}{||\Sigma\boldsymbol{u}||\,||\delta\boldsymbol{u}\times\delta\boldsymbol{\omega}||}. \tag{5.5}$$

The PDF is presented for both data sets in fig. 10. Note that an extra separation at $r = 4.7\lambda$ (the maximum separation attainable using the sub-cubes extracted from the JHU database) is presented for further insight. As required by eq. (5.4) to maintain dissipation downscale, the alignment is found to be biased towards positive values of $\cos\theta$ for all separations such that $\overline{\cos\theta} > 0$. The distributions appear approximately quadratic in nature, with an inflection occurring somewhere between 2.5η and 0.5λ.

As the separation increases, the probability of parallel ($\cos\theta = 1$) and anti-parallel

($\cos\theta = -1$) alignment is increasingly likely. Most evident from the JHU distributions (fig. 10(b)), the increase in likelihood across separations is more rapid for anti-parallel alignment than parallel alignment. A linear regression for these points with increasing scale indicates they will be equal in probability at $r \approx 13\lambda$, corresponding almost exactly to the integral scale of the DNS data set (figure 10(c)). This implies that at $r = L$ the PDF will be symmetric about zero and, due to the parabolic shape, with equal likelihood of parallel and anti-parallel alignment, a minimum at $\cos\theta = 0$, and $\overline{\cos\theta} = 0$. A similar extrapolation for the experimental data was not conclusive due to the limited number of available separations.

6. Conclusions

A scale-space framework, already well established for generalisation of the turbulent energy transfers via the KHMH equation (Hill 2002; Valente & Vassilicos 2015), has been extended analogously to the scale-space helicity and enstrophy together for the first time. This has provided a novel framework for insight on the instantaneous turbulence dynamics that are responsible for establishing the statistically steady state. To exemplify this framework, an analysis of the various inter-scale and inter-space transfers of energy, helicity, and enstrophy in two homogeneous turbulent flows focusing on scales up to the Taylor microscale has been presented.

The correlation-based analysis has revealed that the random sweeping effect is indeed present within all three considered budgets. This was identified through the significant anti-correlation of the unsteady and physical-space transport terms ($\mathcal{A}_t$ and $\mathcal{T}$, respectively) within the individual budgets. A significant correlation of these transfers *between* budgets was also identified via the energy and enstrophy, suggesting that random sweeping also occurs simultaneously *across* budgets. In addition, the energy and enstrophy transfers were also found to correlate through the generation/dissipation of enstrophy and dissipation of energy, consistent with previous studies (Davidson *et al.* 2008). This again points to the connection of mechanisms across budgets.

The anti-correlation between the pressure transport and non-linear inter-scale transfer terms (Π and $\mathcal{T}_p$, respectively), already reported by Yasuda & Vassilicos (2018) in the context of the energy cascade, was also observed in the helicity cascade. In contrast to the energy cascade, this anti-correlation was strongest at the dissipative scales, where both vortex-stretching and twisting mechanisms correlate equally. Overall (i.e. on average) it was found that the downscale helicity cascade couples with expanding pressure forces and the upscale helicity cascade associates with compressing pressure forces.

As a direct consequence of the non-positive definiteness of helicity, it was found that the terms governing the transfers of helicity were entirely decorrelated from those governing the energy and enstrophy. Despite this, it was shown that the scale-to-scale helicity itself influences the energy transfers. On the basis of kinematic arguments, it was demonstrated that the alignment between the two-point velocity sum and the cross product of the velocity and vorticity increments is connected to the overall inter-scale transfer of energy (eq. (5.4)). This is at odds with theoretical independence of small-scale dynamics from large-scale motions, but is consistent with so-called large scale intermittency phenomena observed in numerous studies (e.g. Sreenivasan & Antonia 1997; Blum *et al.* 2010; Carter & Coletti 2018). It is further seen that, to maintain the dissipation of energy, this alignment is non-zero and positive on average.

Taken together, the present work illustrates how the the extended scale-space framework (introduced here in its most general form) can be used to probe the various mechanisms involved in the concurrent exchanges of energy, enstrophy and helicity. In this first iteration, this framework was applied to homogeneous turbulence, allowing us to identify links and similarities between the various transfers. Furthermore, by dissecting the term associated with inter-scale energy exchanges, we find that the scale helicity regulates the imbalance between inter-scale exchanges of large-scale energy (Σq^2) and the inter-space exchanges of small-scale energy (δq^2) through $\Sigma \boldsymbol{u} \cdot (\delta \boldsymbol{\omega} \times \delta \boldsymbol{u})$.

Future applications of the present framework to other canonical problems, such as a Taylor-Green vortex, but also (and perhaps more importantly) to flows where the turbulence is markedly inhomogeneous, such as wall-bounded and free-shear flows, are warranted. A detailed analysis of the scale-space triple product, particularly as it pertains to the large scale sweeping motions (e.g. a conditional analysis for when u_k and u'_k are aligned/anti-aligned) is also low-hanging fruit. Finally, the use of physics-driven instantaneous correlations (as in the present study) as parameters in the loss functions of neural networks for sub-grid stress models in LES is a promising avenue for future research.

Acknowledgements

The authors wish to acknowledge J. Dawson for kindly sharing experimental data. D.W.C. wishes to thank F. Coletti, A. Alexakis, and B. Ganapathisubramani for support in early stages. This work is the product of exchanges of ideas at the Eleventh International Symposium on Turbulence and Shear Flow Phenomena in Southampton, UK.

Data Availability

Data for all figures are available from the University of Southampton repository at https://doi.org/10.5258/SOTON/D2420

Competing Interest

The authors report no conflict of interest.

Appendix A. Energy, enstrophy, and helicity transfer budgets

The extensive size of the data sets makes tabulating all data points at each location in scale space into a single storage variable prohibitively expensive. For this reason, a limited number of separations were chosen in order to store the relevant information in confined memory.

For each volumetric cube of Cartesian data and for each separation, spheres corresponding to scale-space radius r were positioned at all possible centroid locations on the grid. As the number of possible centroid locations decreases with increasing sphere radius, the number of samples used for calculating statistics decreases as r increases (Camussi *et al.* 1996), leading to increased uncertainty at larger separations (e.g. see the error bars of fig. 3). Statistics (i.e. the first and second moments of the quantities of interest) were calculated by averaging over the sphere. As the grid points did not provide a uniform probing of the sphere, a weighting procedure was adopted to account for the non-uniformity. The number of surface points on the sphere was chosen to be $N_s = 96$, with no significant impact on the results tested with a variety of N_s between 24 and 288. The correlation between two quantities, ζ and ξ, is obtained as

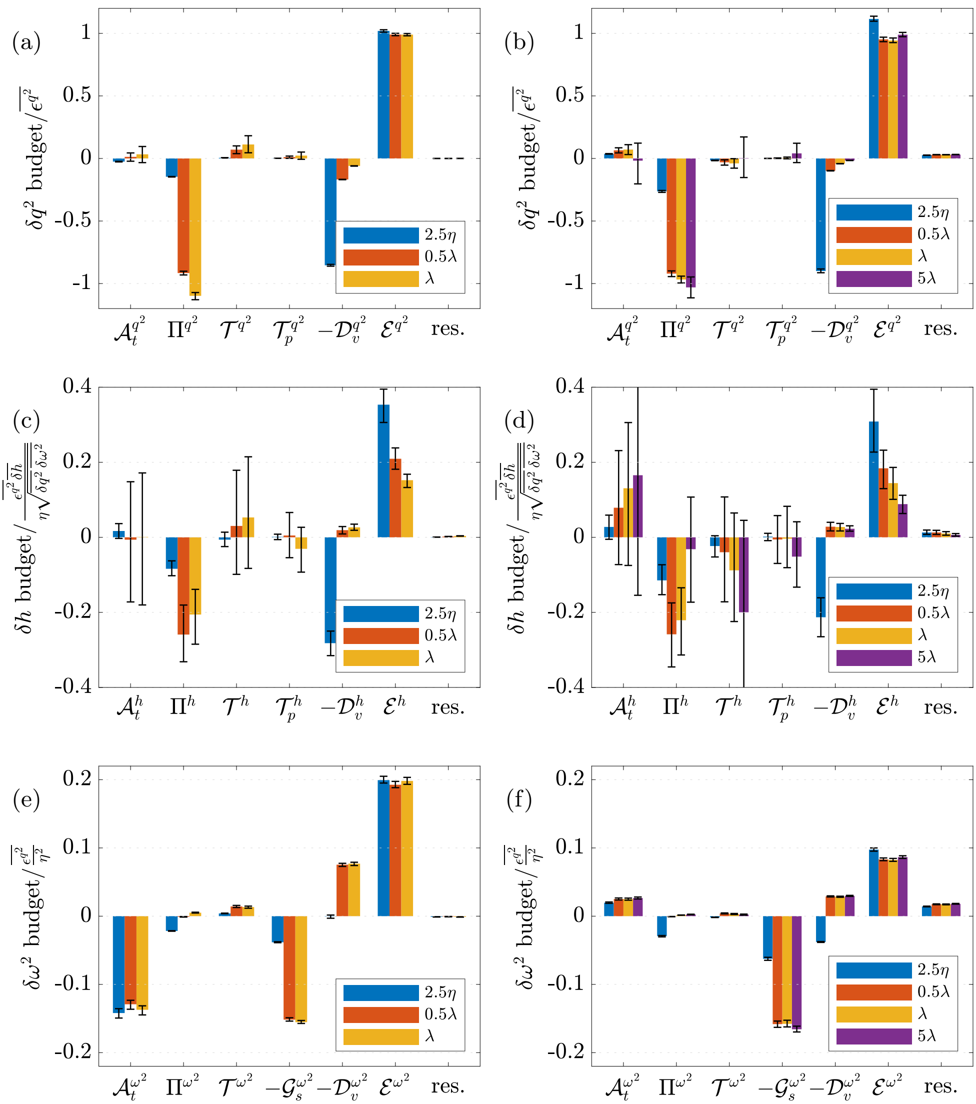

Figure 11: Budgets of terms of eq. (2.4) (a,b), eq. (2.6) (c,d), and eq. (2.8) (e,f) evaluated for VK (a,c,e) and JHU (b,d,f) datasets (res. stands for residuals of the respective budgets).

$$corr(\zeta, \xi) = \frac{\overline{\zeta\xi} - \bar{\zeta}\bar{\xi}}{\sqrt{\overline{\zeta^2} - \bar{\zeta}^2}\sqrt{\overline{\xi^2} - \bar{\xi}^2}}. \tag{A 1}$$

By normalising by the product of the square root of the variance of both quantities a value of 1, 0, and -1 corresponds to perfectly correlated, uncorrelated, and anti-correlated quantities, respectively.

The histogram for each sphere at each separation and for all quantities of interest was tabulated and stored in 2500 linearly spaced bins. Similarly, the joint histogram for each pair of investigated quantities was stored in a 500×500 bin matrix. The large number of bins allowed to capture the most extreme values of the highly intermittent quantities. As these extreme values are not known *a-priori*, an adaptive histogram approach was used in which the bins and bin counts were adjusted when a value exceeding the current limits of the bins was encountered. Once tabulated, the histograms were normalised into PDFs (or joint PDFs).

To validate the adopted approach the budget equations representing the balance of the various inter-scale transfers are presented for the VK and JHU data in fig. 11. Similar results are obtained for both data sets. The energy budgets exhibit the classical behaviour: they are dominated by terms Π^{q^2} and $\mathcal{E}^{q^2}$ at larger separations, while $\mathcal{D}_\nu^{q^2}$ and $\mathcal{E}^{q^2}$ are the most significant as the smallest separation. The accuracy of the method and overall statistics is also supported by the small residuals in each case. However, it must be noted that the particularly small residuals associated with the VK data are largely artificial. The post-processing routine applied to the scanning PIV data yielded the acceleration and pressure fields in addition to the measured velocity fields. This extra information was resolved by minimization of the instantaneous momentum equation residual (i.e. a data assimilation approach). Therefore small values of the budgets residuals are enforced in the case of VK data.

Although there is a generally good match between budgets based on the two data sets, this is certainly not the case when it comes to the unsteady term of the enstrophy budget $\mathcal{A}_t^{\omega^2}$ and enstrophy dissipation rate $\mathcal{E}^{\omega^2}$. The former term ought to vanish in a statistically stationary flow, such as the two considered in this manuscript, yet it dominates the VK enstrophy budget (for the JHU case $\mathcal{A}_t^{\omega^2}$ is indeed small and of the order of the residual). The dissipation term $\mathcal{E}^{\omega^2}$, on the other hand, is twice as large in the VK case than in the JHU data. This mismatch is due to bias error propagation via discrete differentiation. This effect is expected to be the strongest for the enstrophy transfer terms, owing to the high order derivatives involved (acting as noise amplifiers). For example, the measured value of $\mathcal{E}^{\omega^2}$ is proportional to $(\partial\omega_i/\partial x_j)^2_{\text{meas.}} = (\partial\omega_i/\partial x_j)^2_{\text{true}} + 2e(\partial\omega_i/\partial x_j)_{\text{true}} + e^2$, where e represents error. The non-negative term e^2 is the dominating source of bias error (a similar example in the context of the energy dissipation rate is given by Tanaka & Eaton 2007). Since the VK data is the noisier of the two sets, it follows that the measured value of $\mathcal{E}^{\omega^2}$ is larger, in agreement with fig. 11.

Taking into account the above considerations, any conclusions regarding terms $\mathcal{A}_t^{\omega^2}$ and $\mathcal{E}^{\omega^2}$ based on the VK data are questionable. This ambiguity is avoided in the manuscript by discarding the VK data and relying purely on the JHU data for the enstrophy transfers.

Appendix B. Derivation of Triple Product Relation

We start by introducing shorthand notation for the KHMH equation for the energy structure function and the energy sum, respectively:

$$\begin{aligned}\overbrace{\begin{aligned}&\frac{\partial}{\partial t}\delta q^2 + \frac{\partial \delta u_k \delta q^2}{\partial r_k} = -\frac{\partial}{\partial X_k}\Big(\frac{\Sigma u_k \delta q^2}{2}\Big) - \frac{2}{\rho}\frac{\partial \delta u_k \delta p}{\partial X_k}\\ &+\nu\Big[2\frac{\partial^2}{\partial r_k^2} + \frac{1}{2}\frac{\partial^2}{\partial X_k^2}\Big]\delta q^2 - 2\nu\Big[\Big(\frac{\partial u_i}{\partial x_k}\Big)^2 + \Big(\frac{\partial u_i'}{\partial x_k'}\Big)^2\Big]\end{aligned}}^{\mathcal{A}_t^{q^2<} + \Pi^{q^2<} = -\mathcal{T}^{q^2<} - \mathcal{T}_p^{q^2<} + \mathcal{D}_\nu^{q^2<} - \mathcal{E}^{q^2}}\end{aligned} \tag{B 1}$$

$$\overbrace{\frac{\partial}{\partial t}\Sigma q^2 + \frac{\partial \delta u_k \Sigma q^2}{\partial r_k} = -\frac{\partial}{\partial X_k}\Big(\frac{\Sigma u_k \Sigma q^2}{2}\Big) - \frac{2}{\rho}\frac{\partial \Sigma u_k \delta p}{\partial X_k}}^{\mathcal{A}_t^{q^2>} + \Pi^{q^2>} = -\mathcal{T}^{q^2>} - \mathcal{T}_p^{q^2>} + \mathcal{D}_\nu^{q^2>} - \mathcal{E}^{q^2}}$$
$$+\nu\Big[2\frac{\partial^2}{\partial r_k^2} + \frac{1}{2}\frac{\partial^2}{\partial X_k^2}\Big]\Sigma q^2 - 2\nu\Big[\Big(\frac{\partial u_i}{\partial x_k}\Big)^2 + \Big(\frac{\partial u_i'}{\partial x_k'}\Big)^2\Big]. \tag{B 2}$$

Simplification starts with the Lamb decomposition applied to the non-linear terms. This can begin with the non-linear terms of either eq. (B 1) or eq. (B 2) and leads to the same result:

$$\begin{aligned}
&\overbrace{2\delta u_i\big(u_j\frac{\partial}{\partial x_j}u_i - u_j'\frac{\partial}{\partial x_j'}u_i'\big)}^{\mathcal{T}^{q^2<} + \Pi^{q^2<}}\\
&= 2\delta u_i\Big(\epsilon_{kji}\omega_k u_j - \epsilon_{kji}\omega_k' u_j' + \frac{1}{2}\frac{\partial}{\partial x_i}(u_j u_j) - \frac{1}{2}\frac{\partial}{\partial x_i'}(u_j' u_j')\Big)\\
&= 2\delta u_i\epsilon_{kji}\Big(\delta\omega_k\Sigma u_j + \omega_k' u_j - \omega_k u_j'\Big) + 2\delta u_i\Big(\frac{1}{2}\frac{\partial}{\partial x_i}(u_j u_j) - \frac{1}{2}\frac{\partial}{\partial x_i'}(u_j' u_j')\Big)\\
&= -2\Sigma u_j\epsilon_{kij}\delta\omega_k\delta u_i + 2\delta u_i\epsilon_{kji}(\omega_k' u_j - \omega_k u_j')\\
&\quad +2\delta u_i\Big(\frac{1}{2}\frac{\partial}{\partial x_i}(u_j u_j) - \frac{1}{2}\frac{\partial}{\partial x_i'}(u_j' u_j')\Big)\\
&= -2\Sigma u_j\epsilon_{kij}\delta\omega_k\delta u_i + 2\delta u_i\epsilon_{kji}\epsilon_{mlk}(u_j\frac{\partial}{\partial x_m'}u_l' - u_j'\frac{\partial}{\partial x_m}u_l)\\
&\quad +2\delta u_i\Big(\frac{1}{2}\frac{\partial}{\partial x_i}(u_j u_j) - \frac{1}{2}\frac{\partial}{\partial x_i'}(u_j' u_j')\Big)\\
&= -2\Sigma u_j\epsilon_{kij}\delta\omega_k\delta u_i + 2\delta u_i(\delta_{jm}\delta_{il} - \delta_{jl}\delta_{im})(u_j\frac{\partial}{\partial x_m'}u_l' - u_j'\frac{\partial}{\partial x_m}u_l)\\
&\quad +2\delta u_i\Big(\frac{1}{2}\frac{\partial}{\partial x_i}(u_j u_j) - \frac{1}{2}\frac{\partial}{\partial x_i'}(u_j' u_j')\Big)\\
&= -2\Sigma u_j\epsilon_{kij}\delta\omega_k\delta u_i + 2\delta u_i(u_j\frac{\partial}{\partial x_j'}u_i' - u_j'\frac{\partial}{\partial x_j}u_i)\\
&\quad +2\delta u_i\Big(-u_j\frac{\partial}{\partial x_i'}u_j' + u_j'\frac{\partial}{\partial x_i}u_j + \frac{1}{2}\frac{\partial}{\partial x_i}(u_j u_j) - \frac{1}{2}\frac{\partial}{\partial x_i'}(u_j' u_j')\Big)\\
&= -2\Sigma u_j\epsilon_{kij}\delta\omega_k\delta u_i + 2\delta u_i(-u_j\frac{\partial}{\partial x_j'}\delta u_i - u_j'\frac{\partial}{\partial x_j}\delta u_i) + \delta u_i(\frac{\partial}{\partial x_i}\Sigma q^2 - \frac{\partial}{\partial x_i'}\Sigma q^2)\\
&= \overbrace{-2\Sigma u_j\epsilon_{kij}\delta\omega_k\delta u_i}^{-2\Sigma\boldsymbol{u}\cdot(\delta\boldsymbol{\omega}\times\delta\boldsymbol{u})} + \overbrace{\frac{\partial}{\partial r_j}(\delta u_j\delta q^2)}^{+\Pi^{q^2<}} - \overbrace{\frac{1}{2}\frac{\partial}{\partial X_j}(\Sigma u_j\delta q^2)}^{-\mathcal{T}^{q^2<}} + \overbrace{2\frac{\partial}{\partial r_j}(\delta u_j\Sigma q^2)}^{+2\Pi^{q^2>}}
\end{aligned} \tag{B 3}$$

The final expression in shorthand notation is

$$\mathcal{T}^{q^2<} + \Pi^{q^2<} = -2\Sigma\boldsymbol{u}\cdot(\delta\boldsymbol{\omega}\times\delta\boldsymbol{u}) + \Pi^{q^2<} - \mathcal{T}^{q^2<} + 2\Pi^{q^2>}. \tag{B 4}$$

Subtracting $\Pi^{q^2<}$ from both sides, dividing by two, and rearranging we arrive at eq. (5.3).

REFERENCES

Alexakis, Alexandros 2017 Helically decomposed turbulence. *Journal of Fluid Mechanics* **812**, 752–770.

Alexakis, Alexandros & Biferale, Luca 2018 Cascades and transitions in turbulent flows. *Physics Reports* **767**, 1–101.

Alexakis, Alexandros & Chibbaro, Sergio 2020 Local energy flux of turbulent flows. *Phys. Rev. Fluids* **5**, 094604.

Alves Portela, F, Papadakis, G & Vassilicos, JC 2017 The turbulence cascade in the near wake of a square prism. *Journal of Fluid Mechanics* **825**, 315–352.

Arun, S., Sameen, A., Srinivasan, Balaji & Girimaji, Sharath S. 2021 Scale-space energy density function transport equation for compressible inhomogeneous turbulent flows. *Journal of Fluid Mechanics* **920**, A31.

Bershadskii, A, Kit, E, Tsinober, A & Vaisburd, H 1994 Strongly localized events of energy, dissipation, enstrophy and enstrophy generation in turbulent flows. *Fluid dynamics research* **14** (2), 71.

Biferale, L, Musacchio, Stefano & Toschi, F 2013 Split energy-helicity cascades in three-dimensional homogeneous and isotropic turbulence .

Blum, Daniel B, Kunwar, Surendra B, Johnson, James & Voth, Greg A 2010 Effects of nonuniversal large scales on conditional structure functions in turbulence. *Physics of Fluids* **22** (1), 015107.

Boffetta, Guido & Ecke, Robert E 2012 Two-dimensional turbulence. *Annual review of fluid mechanics* **44**, 427–451.

Bos, Wouter JT 2021 Three-dimensional turbulence without vortex stretching. *Journal of Fluid Mechanics* **915**.

Brissaud, A, Frisch, Uriel, Léorat, Jacques, Lesieur, Marcel & Mazure, Alain 1973 Helicity cascades in fully developed isotropic turbulence. *Physics of Fluids* **16** (8), 1366–1367.

Camussi, R, Baudet, C, Benzi, R & Ciliberto, S 1996 Statistical uncertainty in the analysis of structure functions in turbulence. *Physical Review E* **54** (4), R3098.

Carbone, Maurizio & Bragg, Andrew D 2020 Is vortex stretching the main cause of the turbulent energy cascade? *Journal of Fluid Mechanics* **883**.

Carter, Douglas W & Coletti, Filippo 2018 Small-scale structure and energy transfer in homogeneous turbulence. *Journal of Fluid Mechanics* **854**, 505–543.

Chen, Qiaoning, Chen, Shiyi & Eyink, Gregory L 2003 The joint cascade of energy and helicity in three-dimensional turbulence. *Physics of Fluids* **15** (2), 361–374.

Chien, Chen-Chi, Blum, Daniel B & Voth, Greg A 2013 Effects of fluctuating energy input on the small scales in turbulence. *Journal of fluid mechanics* **737**, 527–551.

Chkhetiani, OG 1996 On the third moments in helical turbulence. *Journal of Experimental and Theoretical Physics Letters* **63** (10), 808–812.

Cimarelli, Andrea, De Angelis, Elisabetta, Jimenez, Javier & Casciola, Carlo Massimo 2016 Cascades and wall-normal fluxes in turbulent channel flows. *Journal of Fluid Mechanics* **796**, 417–436.

Danaila, L, Krawczynski, JF, Thiesset, F & Renou, B 2012 Yaglom-like equation in axisymmetric anisotropic turbulence. *Physica D: Nonlinear Phenomena* **241** (3), 216–223.

Dascaliuc, R & Grujić, Z 2013 Coherent vortex structures and 3d enstrophy cascade. *Communications in Mathematical Physics* **317** (2), 547–561.

Davidson, PA, Morishita, K & Kaneda, Y 2008 On the generation and flux of enstrophy in isotropic turbulence. *Journal of Turbulence* (9), N42.

Davidson, PA & Pearson, BR 2005 Identifying turbulent energy distributions in real, rather than fourier, space. *Physical review letters* **95** (21), 214501.

Deusebio, Enrico, Boffetta, Guido, Lindborg, Erik & Musacchio, Stefano 2014 Dimensional transition in rotating turbulence. *Physical Review E* **90** (2), 023005.

Elsinga, GE, Ishihara, T, Goudar, MV, Da Silva, CB & Hunt, JCR 2017 The scaling of straining motions in homogeneous isotropic turbulence. *Journal of Fluid Mechanics* **829**, 31–64.

Eyink, Gregory L 1996 Exact results on stationary turbulence in 2d: consequences of vorticity conservation. *Physica D: Nonlinear Phenomena* **91** (1-2), 97–142.

Falkovich, Gregory 2009 Symmetries of the turbulent state. *Journal of Physics A: Mathematical and Theoretical* **42** (12), 123001.

Falkovich, Gregory, Boffetta, G, Shats, Michael & Lanotte, AS 2017 Introduction to focus issue: two-dimensional turbulence.

Fjørtoft, Ragnar 1953 On the changes in the spectral distribution of kinetic energy for twodimensional, nondivergent flow. *Tellus* **5** (3), 225–230.

Gatti, Davide, Chiarini, Alessandro, Cimarelli, Andrea & Quadrio, Maurizio 2020 Structure function tensor equations in inhomogeneous turbulence. *Journal of Fluid Mechanics* **898**.

Germano, Massimo, Piomelli, Ugo, Moin, Parviz & Cabot, William H 1991 A dynamic subgrid-scale eddy viscosity model. *Physics of Fluids A: Fluid Dynamics* **3** (7), 1760–1765.

Gomes-Fernandes, R, Ganapathisubramani, B & Vassilicos, JC 2015 The energy cascade in near-field non-homogeneous non-isotropic turbulence. *Journal of Fluid Mechanics* **771**, 676–705.

Goto, Susumu & Vassilicos, JC 2016 Unsteady turbulence cascades. *Physical Review E* **94** (5), 053108.

Hill, Reginald J 2002 Exact second-order structure-function relationships. *Journal of Fluid Mechanics* **468**, 317–326.

Hosokawa, Iwao 2007 A paradox concerning the refined similarity hypothesis of kolmogorov for isotropic turbulence. *Progress of Theoretical Physics* **118** (1), 169–173.

Inagaki, Kazuhiro 2021 Scale-similar structures of homogeneous isotropic non-mirror-symmetric turbulence based on the lagrangian closure theory. *Journal of Fluid Mechanics* **926**.

Ishihara, Takashi, Gotoh, Toshiyuki & Kaneda, Yukio 2009 Study of high–reynolds number isotropic turbulence by direct numerical simulation. *Annual Review of Fluid Mechanics* **41**, 165–180.

Ishihara, Takashi, Kaneda, Yukio & Hunt, Julian CR 2013 Thin shear layers in high reynolds number turbulence—dns results. *Flow, turbulence and combustion* **91** (4), 895–929.

Jiménez, Javier, Wray, Alan A, Saffman, Philip G & Rogallo, Robert S 1993 The structure of intense vorticity in isotropic turbulence. *Journal of Fluid Mechanics* **255**, 65–90.

van Kan, Adrian & Alexakis, Alexandros 2022 Energy cascades in rapidly rotating and stratified turbulence within elongated domains. *Journal of Fluid Mechanics* **933**.

Kivotides, Demosthenes & Leonard, Anthony 2021 Helicity spectra and topological dynamics of vortex links at high reynolds numbers. *Journal of Fluid Mechanics* **911**.

Kleckner, Dustin, Kauffman, Louis H & Irvine, William TM 2016 How superfluid vortex knots untie. *Nature Physics* **12** (7), 650–655.

Knutsen, Anna N, Baj, Pawel, Lawson, John M, Bodenschatz, Eberhard, Dawson, James R & Worth, Nicholas A 2020 The inter-scale energy budget in a von kármán mixing flow. *Journal of Fluid Mechanics* **895**.

Kolmogorov, Andrey Nikolaevich 1941*a* Dissipation of energy in locally isotropic turbulence. In *Dokl. Akad. Nauk SSSR*, , vol. 32, pp. 16–18.

Kolmogorov, Andrey Nikolaevich 1941*b* The local structure of turbulence in incompressible viscous fluid for very large reynolds numbers. In *Dokl. Akad. Nauk SSSR*, , vol. 30, pp. 299–303.

Kraichnan, Robert H 1967 Inertial ranges in two-dimensional turbulence. *The Physics of Fluids* **10** (7), 1417–1423.

Kraichnan, Robert H 1973 Helical turbulence and absolute equilibrium. *Journal of Fluid Mechanics* **59** (4), 745–752.

Kraichnan, Robert H 1974 On kolmogorov's inertial-range theories. *Journal of Fluid Mechanics* **62** (2), 305–330.

Kurien, Susan, Taylor, Mark A & Matsumoto, Takeshi 2004 Isotropic third-order statistics in turbulence with helicity: the 2/15-law. *arXiv preprint nlin/0409030* .

LAI, CHRIS CK, CHARONKO, JOHN J & PRESTRIDGE, KATHERINE 2018 A kármán-howarth-monin equation for variable-density turbulence. *Journal of Fluid Mechanics* **843**, 382.

LAVAL, JP, DUBRULLE, B & NAZARENKO, S 2001 Nonlocality and intermittency in three-dimensional turbulence. *Physics of Fluids* **13** (7), 1995–2012.

LAWSON, JM & DAWSON, JR 2015 On velocity gradient dynamics and turbulent structure. *Journal of Fluid Mechanics* **780**, 60–98.

LAWSON, JOHN M & DAWSON, JAMES R 2014 A scanning piv method for fine-scale turbulence measurements. *Experiments in fluids* **55** (12), 1–19.

LEVICH, E & SHTILMAN, L 1988 Coherence and large fluctuations of helicity in homogeneous turbulence. *Physics Letters A* **126** (4), 243–248.

LI, YI, PERLMAN, ERIC, WAN, MINPING, YANG, YUNKE, MENEVEAU, CHARLES, BURNS, RANDAL, CHEN, SHIYI, SZALAY, ALEXANDER & EYINK, GREGORY 2008 A public turbulence database cluster and applications to study lagrangian evolution of velocity increments in turbulence. *Journal of Turbulence* (9), N31.

LINDBORG, ERIK 2007 Third-order structure function relations for quasi-geostrophic turbulence. *Journal of Fluid Mechanics* **572**, 255–260.

LINDBORG, ERIK & NORDMARK, ARNE 2022 Two-dimensional turbulence on a sphere. *Journal of Fluid Mechanics* **933**, A60.

L'VOV, VICTOR S, PODIVILOV, EVGENII & PROCACCIA, ITAMAR 1997 Exact result for the 3rd order correlations of velocity in turbulence with helicity. *arXiv preprint chao-dyn/9705016* .

MARATI, N, CASCIOLA, CM & PIVA, R 2004 Energy cascade and spatial fluxes in wall turbulence. *Journal of Fluid Mechanics* **521**, 191–215.

MININNI, PD, ALEXAKIS, A & POUQUET, ANNICK 2006 Large-scale flow effects, energy transfer, and self-similarity on turbulence. *Physical Review E* **74** (1), 016303.

MOFFATT, HK & TSINOBER, A 1992 Helicity in laminar and turbulent flow. *Annual review of fluid mechanics* **24** (1), 281–312.

MOFFATT, HENRY KEITH 1969 The degree of knottedness of tangled vortex lines. *Journal of Fluid Mechanics* **35** (1), 117–129.

MOLLICONE, J-P, BATTISTA, F, GUALTIERI, P & CASCIOLA, CM 2018 Turbulence dynamics in separated flows: The generalised kolmogorov equation for inhomogeneous anisotropic conditions. *Journal of Fluid Mechanics* **841**, 1012–1039.

MONIN, AS & YAGLOM, AO M 1975 Statistical fluid mechanics, vol. 2.

MOREAU, JEAN JACQUES 1960 Constantes d'un îlot tourbillonnaire en fluide parfait barotrope. *Comptes rendus hebdomadaires des séances de l'Académie des sciences* **252**, 2810–2812.

NOVARA, MATTEO & SCARANO, FULVIO 2013 A particle-tracking approach for accurate material derivative measurements with tomographic piv. *Experiments in fluids* **54** (8), 1–12.

PELZ, RICHARD B, YAKHOT, VICTOR, ORSZAG, STEVEN A, SHTILMAN, LEONID & LEVICH, EVGENY 1985 Velocity-vorticity patterns in turbulent flow. *Physical review letters* **54** (23), 2505.

POPE, STEPHEN B 2001 Turbulent flows.

POUQUET, ANNICK, ROSENBERG, DUANE, STAWARZ, JULIA E & MARINO, RAFFAELE 2019 Helicity dynamics, inverse, and bidirectional cascades in fluid and magnetohydrodynamic turbulence: a brief review. *Earth and Space Science* **6** (3), 351–369.

RAYNAL, FLORENCE 1996 Exact relation between spatial mean enstrophy and dissipation in confined incompressible flows. *Physics of Fluids* **8** (8), 2242–2244.

RICHARDSON, LEWIS FRY 1920 The supply of energy from and to atmospheric eddies. *Proceedings of the Royal Society of London. Series A, Containing Papers of a Mathematical and Physical Character* **97** (686), 354–373.

SCOTT, ROBERT B & WANG, FAMING 2005 Direct evidence of an oceanic inverse kinetic energy cascade from satellite altimetry. *Journal of Physical Oceanography* **35** (9), 1650–1666.

SIGGIA, ERIC D 1981 Numerical study of small-scale intermittency in three-dimensional turbulence. *Journal of Fluid Mechanics* **107**, 375–406.

SREENIVASAN, KATEPALLI R 1995 On the universality of the kolmogorov constant. *Physics of Fluids* **7** (11), 2778–2784.

SREENIVASAN, KATEPALLI R & ANTONIA, RA 1997 The phenomenology of small-scale turbulence. *Annual review of fluid mechanics* **29** (1), 435–472.

Stepanov, Rodion, Golbraikh, Ephim, Frick, Peter & Shestakov, Alexander 2015 Hindered energy cascade in highly helical isotropic turbulence. *Physical Review Letters* **115** (23), 234501.

Tanaka, Tomohiko & Eaton, John K 2007 A correction method for measuring turbulence kinetic energy dissipation rate by piv. *Experiments in Fluids* **42** (6), 893–902.

Tennekes, Hendrik & Lumley, John L 2018 *A first course in turbulence*. MIT press.

Tsinober, Arkady 2001 *An informal introduction to turbulence*, , vol. 63. Springer Science & Business Media.

Valente, PC & Vassilicos, JC 2015 The energy cascade in grid-generated non-equilibrium decaying turbulence. *Physics of Fluids* **27** (4), 045103.

Van Atta, CW & Antonia, RA 1980 Reynolds number dependence of skewness and flatness factors of turbulent velocity derivatives. *The Physics of Fluids* **23** (2), 252–257.

Von Karman, Theodore & Howarth, Leslie 1938 On the statistical theory of isotropic turbulence. *Proceedings of the Royal Society of London. Series A-Mathematical and Physical Sciences* **164** (917), 192–215.

Waleffe, Fabian 1992 The nature of triad interactions in homogeneous turbulence. *Physics of Fluids A: Fluid Dynamics* **4** (2), 350–363.

Wang, ChengYue, Gao, Qi, Wei, RunJie, Li, Tian & Wang, JinJun 2017 Weighted divergence correction scheme and its fast implementation. *Experiments in Fluids* **58** (5), 44.

Yan, Zheng, Li, Xinliang, Yu, Changping, Wang, Jianchun & Chen, Shiyi 2020 Dual channels of helicity cascade in turbulent flows. *Journal of Fluid Mechanics* **894**.

Yasuda, Tatsuya & Vassilicos, John Christos 2018 Spatio-temporal intermittency of the turbulent energy cascade. *Journal of Fluid Mechanics* **853**, 235–252.

Yeung, PK & Brasseur, James G 1991 The response of isotropic turbulence to isotropic and anisotropic forcing at the large scales. *Physics of Fluids A: Fluid Dynamics* **3** (5), 884–897.

Yokoi, Nobumitsu & Yoshizawa, Akira 1993 Statistical analysis of the effects of helicity in inhomogeneous turbulence. *Physics of Fluids A: Fluid Dynamics* **5** (2), 464–477.

Zhou, Ye 2021 Turbulence theories and statistical closure approaches. *Physics Reports* **935**, 1–117.

Zhou, Yi, Nagata, Kouji, Sakai, Yasuhiko, Ito, Yasumasa & Hayase, Toshiyuki 2016 Spatial evolution of the helical behavior and the 2/3 power-law in single-square-grid-generated turbulence. *Fluid Dynamics Research* **48** (2), 021404.

Zimmerman, Spencer J, Antonia, RA, Djenidi, L, Philip, J & Klewicki, JC 2022 Approach to the 4/3 law for turbulent pipe and channel flows examined through a reformulated scale-by-scale energy budget. *Journal of Fluid Mechanics* **931**.